THE UNIVERSITY of EDINBURGH

Edinburgh Research Explorer

Pre/pro-B cells generate macrophage populations during homeostasis and inflammation

Citation for published version:
Audzevich, T, Bashford-rogers, R, Mabbott, NA, Frampton, D, Freeman, TC, Potocnik, A, Kellam, P & Gilroy, DW 2017, 'Pre/pro-B cells generate macrophage populations during homeostasis and inflammation', *Proceedings of the National Academy of Sciences (PNAS)*, vol. 114, no. 20, pp. E3954-E3963. https://doi.org/10.1073/pnas.1616417114

Digital Object Identifier (DOI):
10.1073/pnas.1616417114

Link:
Link to publication record in Edinburgh Research Explorer

Document Version:
Peer reviewed version

Published In:
Proceedings of the National Academy of Sciences (PNAS)

Publisher Rights Statement:
Freely available online through the PNAS open access option.

General rights
Copyright for the publications made accessible via the Edinburgh Research Explorer is retained by the author(s) and / or other copyright owners and it is a condition of accessing these publications that users recognise and abide by the legal requirements associated with these rights.

Take down policy
The University of Edinburgh has made every reasonable effort to ensure that Edinburgh Research Explorer content complies with UK legislation. If you believe that the public display of this file breaches copyright please contact openaccess@ed.ac.uk providing details, and we will remove access to the work immediately and investigate your claim.

OPEN ACCESS

Download date: 07. May. 2023

Novel pre/pro-B cells generates macrophage populations during homeostasis and inflammation

[1]Tatsiana Audzevich, [2]Rachael Bashford-Rogers, [3]Neil A. Mabbott, [4]Dan Frampton, [3]Tom C. Freeman, [5]Alexandre J. Potocnik, [2]Paul Kellam and [1]Derek W. Gilroy

[1]Centre for Clinical Pharmacology and Therapeutics, Division of Medicine, 5 University Street, University College London, London WC1E 6JJ, United Kingdom.

[2]Department of Medicine, University of Cambridge, Cambridge Biomedical Campus, Hills Road, Cambridge, CB2 0XY, UK.

[3]The Roslin Institute & Royal (Dick) School of Veterinary Sciences, University of Edinburgh, Easter Bush, Midlothian, EH25 9RG, United Kingdom.

[4]Division of Infection and Immunity, University College London, London WC1E 6AE, United Kingdom.

[5]Insitute of Immunology and Infection Research, University of Edinburgh, Edinburgh EH9 3FL, United Kingdom

Corresponding author: Derek W Gilroy: d.gilroy@ucl.ac.uk

Short title: Novel source of tissue macrophages

Category: Biological Sciences, Cell biology

Keywords: Phagocytes, Haematopoiesis, Host defence

ABSTRACT

Most tissue-resident macrophages (Mφs) are believed to be derived prenatally and assumed to maintain themselves throughout life by self-proliferation. However, in adult mice we identified a novel progenitor within bone marrow early pro-B cell/fraction B that differentiates into tissue Mφs. These Mφ precursors have non-rearranged BCR genes and co-express myeloid (GR1, CD11b and CD16/32) and lymphoid (B220 and CD19) lineage markers. During steady state these precursors exit bone marrow losing Gr1 and enter systemic circulation seeding the gastrointestinal system as well as pleural and peritoneal cavities but not the brain. Whilst in these tissues they acquire a transcriptome identical to embryonically derived tissue-resident Mφs. Similarly, these Mφ precursors also enter sites of inflammation gaining CD115, F4/80 and CD16/32 and become indistinguishable from blood monocyte-derived Mφs. Thus, we have identified a population of cells within bone marrow early pro-B cell compartment that possess functional platicity to differentiate into either tissue-resident or inflammatory Mφs depending on micro-environmental signals. We propose that these precursors represent an additional source of Mφ populations in adult mice during steady state and inflammation.

SIGNIFICANCE STATEMENT

In this report we provide evidence of a novel source of macrophage populations that are derived from a unique bi-phenotypic early pro-B cells with non-re-arranged BCR. These early precursors give rise to either tissue resident- or monocyte-derived macrophages during homeostasis and inflammatory responses thereby demonstrating functional plasticity depending on the environmental cues in adult mice. We suggest that these data significantly advance and expand our understanding of Mφ biology and haematopoiesis, the plasticity of hematopoietic precursors and the heterogeneity of Mφ subsets.

\body

INTRODUCTION

Monocytes and Mφs maintain tissue homeostasis and orchestrate immune mediated responses to infection/injury. During embryonic haematopoiesis monocytes arise from myeloid precursors in foetal liver while during adulthood they are derived from bone marrow progenitors. Circulating monocytes migrate to sites of infection/injury where they differentiate into Mφs(1, 2) and under certain circumstances can also replenish Mφs in the colon(3). In contrast, the majority of resident Mφ populations are embryonically derived and are proposed to maintain their numbers by local proliferation after birth(4-9). However, in the course of our studies we identified a population of biphenotypic Mφs in the serous cavities of naive mice that co-express the B lineage marker CD19 and the Mφ markers CD11b and F4/80. Interestingly, revised models of haematopoiesis(10, 11) and evidence of developmental plasticity within haematopoietic precursors suggest a closer developmental relationship between myeloid and lymphoid lineages than previously appreciated(10-14). Consequently, as there is convincing evidence that lymphocyte-to-Mφ differentiation can occur in vitro under artificial experimental settings(15-19), we determined whether the biphenotypic cells we observed in the peritoneal and pleural cavities as well as the gastrointestinal system were derived from B-lymphocytes or precursors within the B cell lineage. If so, this would challenge the existing view that local self-proliferation is the only means by which tissue-resident Mφs maintain their numbers throughout adulthood.

Using a range of B cell lineage-specific transgenic reporter mice as well as single cell PCR, ImageStream/polychromatic flow cytometry and adoptive transfer studies, our data show that contrary to previous publications(16, 18, 19) mature B cells do not differentiate into Mφs. Instead, we found a population of cells within the early pro-B cell/fraction B cell compartment with non-rearranged BCR genes that exit bone marrow under steady state, circulate in peripheral blood and populate serous cavities where they differentiate into Mφs thereby contributing to the overall pool of tissue Mφs alongside embryonically-derived cells. Hence, in addition to local proliferation, we now further refine our understanding of how tissue Mφs numbers are maintained during adulthood.

Moreover, these data report a novel cell with origins that are morphogenically distinct from embryonic Mφ precursors, but that nonetheless differentiate in to cells with equivalent phenotypes.

RESULTS

Mφs with a potential B cell origin detected using *Mb1*-iCre/Rosa26R-*YFP* reporter mice

Analysis of cells from the peritoneal cavity of naïve wild-type mice revealed a population of F4/80^{++}CD11b^{++} Mφs that also expressed CD19 (**Fig. 1A**). These cells constitute ~0.8% of total Mφs suggesting a potential developmental relationship between mononuclear phagocytes and B cells. Crossing *Mb1*-iCre(20) with Rosa26-*YFP*(21) mice allowed us to investigate this potential further as *Mb1*-dependent Cre-recombinase expression is induced in B cells during the very early pro-B stage(20). Thus, tissue Mφs that express YFP will have been derived from B cells. In naive *Mb1*-iCre/Rosa26-*YFP* mice a significant proportion of Mφs expressed YFP including ~25% of peritoneal Mφs, 4-10% of pleural cavity Mφs and 1-2.5% of intestinal Mφs, with very few YFP^{+} Mφs detectable in the spleen, liver and brain (**Fig. 1B**); gating strategies to discern tissue Mφ populations are shown in **supplementary Fig. 1.1.**

To determine B cell lineage restricted reporter expression in *Mb1*-iCre/Rosa26-*YFP* mice we analysed YFP expression in various hematopoietic progenitors of these animals as well as mature leukocytes in various tissue compartments. Analysis revealed that 97-99% of peripheral blood B cells were YFP^{+} with only minimal YFP expression detected on T cells and monocytes with no YFP expression detectable on neutrophils (**supplementary Fig. 1.2A**). In bone marrow we found ~7% of YFP^{+} cells among Lin^{-}IL7Rα^{+}Sca-1^{+}c-Kit^{+} common lymphoid progenitors (CLP), but no YFP^{+} cells was detected among Lin^{-}IL7Rα^{-}CD34$^{+/-}$CD16/32^{+} common myeloid progenitors (CMP). Equally, there was no YFP expression detectable in Lin^{-}IL7Rα^{-}Sca-1^{++}c-Kit^{++} multi-lineage progenitors (MLP) and Lin^{-}IL7Rα^{-}CD34^{+}CD16/32^{++} granulocyte/ Mφs progenitors (GMP) (**supplementary Fig. 1.2B**). More specifically, the lymphoid-biased multipotent progenitor (LMPP, Lin^{-}IL7Rα^{-}Flk-2^{hi}CD34^{+}) was found to be negative (supplementary Fig. 1.2B). Finally, ~0.15% YFP^{+} cells was detected in Lin^{-}CD4^{-}CD8^{-} early thymic progenitors (**supplementary Fig. 1.2C**). Gating strategies for flow cytometric identification of hematopoietic progenitors in bone marrow and T cell progenitors in thymus are shown in **supplementary Figs 1.3 and 1.4**.

Phagocytosis of apoptotic YFP$^+$ B cells by Mφs does not generate YFP$^+$ Mφs

Immunofluorescent microscopy on FACS-purified peritoneal cell populations as well as *in vitro* phagocytosis assays where YFP$^-$ Mφs were co-cultured with early/late apoptotic YFP$^+$ B cells confirmed that the YFP fluorescence detected in YFP$^+$ Mφs from *Mb1*-iCre/Rosa26-*YFP* mice was due to the cytoplasmic YFP expression in Mφs and not from ingestion of apoptotic YFP$^+$ B cells (**supplementary Fig 2A-E**).

YFP$^+$ Mφs in *Mb1*-iCre/Rosa26R-*YFP* mice do not arise form mature B cells

Hematopoietic development of B cells includes seven stages (A to C, C' to F), which are defined by stage-specific cell surface marker expression and B cell receptor (BCR) gene rearrangement status(22, 23). Rearrangement of Ig genes, which is initiated during bone marrow development at pro-B cell stage/fraction B stage and completed in pre-B/fraction C' B cells(23) leads to surface expression of BCRs of unique DNA sequence and enables B cell development and survival(24). This distinctive feature of B cell development was exploited to determine whether YFP$^+$ Mφs carry V-DJ re-arrangements in their IgH locus as evidence of their origin from mature/pre B cells.

Before embarking upon single cell PCR to determine whether YFP$^+$ Mφs carry V-DJ re-arrangements we ensured that cell populations we intended to FACSort were single cells and not doublets/clusters of Mφs with YFP$^+$ B cells. Previous studies have reported biphenotypic murine peritoneal Mφs co-expressing F4/80 and CD11b along with surface IgM, CD5, CD19 and/or B220(25-27), but without considering the possibility of cell doublets/clusters generating potential false-positive data. ImageStream analysis of the murine peritoneum identified three distinct cell types within the CD11b^{++}F4/80^{++} Mφ gate including CD19$^-$YFP$^-$ (embryonic Mφs), CD19$^-$YFP$^+$ and CD19$^+$YFP$^+$ cells (**Fig. 2A**). It's this latter biphenotypic Mφ population co-expressing CD11b, F4/80, YFP and CD19 that we suspect are intermediates in the transition of B cells to Mφs. However, ImageStream also revealed significant numbers of doublets (Mφ/B cell clusters) within this intermediate CD19$^+$YFP$^+$ Mφ population, with single biphenotypic cells constituting only ~16.74% of the total CD19$^+$YFP$^+$ Mφs (**Fig. 2B and Table**), meaning that approximately 80% cells within the

biphenotypic population are aggregates of Mφs and B cells. See **supplementary Fig 3.1** for further data on identifying clusters/doublets.

Therefore, we sorted $CD19^{-}YFP^{-}$ (embryonic Mφs), $CD19^{-}YFP^{+}$ and intermediate $CD19^{+}YFP^{+}$ biphenotypic cells along with B cells to act as a positive control bearing in mind that the intermediate or biphenotypic cells contain random clusters of Mφ/B cell aggregates. On a single cell level, while V-DJ re-arrangements were detected in ~71% of single B cells analysed, only ~33% of intermediate $CD19^{+}YFP^{+}$ Mφs were $V\text{-}DJ^{+}$ with no re-arrangements found in $CD19^{-}YFP^{+}$ B cell-derived Mφs or $CD19^{-}YFP^{-}$ tissue-resident embryonic Mφs (**Fig. 2C**). A significant increase in the frequency of $V\text{-}DJ^{+}$ reactions in the $CD19^{+}YFP^{+}$ populations was found, which increased from 33% to 84% (compared to ~87% for B cells) when multiple cells (5, 10 or 20) per reaction were analysed. We propose that this arose from contaminating B cells or B cell/Mφ clusters in at least ~33% of single-sorted B-Mφ intermediate $CD19^{+}YFP^{+}$ Mφs. As expected all single B cells expressed *Cd79b* while $CD19^{-}YFP^{+}$ B cell-derived Mφs and $CD19^{-}YFP^{-}$ tissue-resident embryonic Mφs expressed *Emr1* (encoding the Mφs marker F4/80). Unlike other Mφ subsets, co-expression of the B cell-specific transcript *Cd79b* and the Mφs-specific transcript *Emr1* was detected in intermediate $CD19^{+}YFP^{+}$ Mφs on a single cell level. Collectively, these data show that YFP^{+} macrophages display no evidence of VDJ recombination and that VDJ recombination detected in $CD19^{+}YFP^{+}$ Mφs arises from sorting of doublets/clusters.

Of note, single cell PCR reported doublet rates of ~30% while ImageStream estimated ~80%. This disparity arises from the different algorithms flow cytometry uses for single cell sorting (for PCR) compared to ImageStream. Nonetheless, both methods reliably identified the presence of contaminating B cell/Mφ clusters within the intermediate $CD19^{+}YFP^{+}$ Mφ population, which, in the absence of stringent exclusion criteria, will generate false positive results.

.

Evaluation of B cell-specific reporter mice point toward early pro-B cell origin of YFP$^+$ Mφs

We analysed bone marrow of *Cd19*-Cre/Rosa26-*YFP* mice using the gating strategy in **supplementary Fig. 4.1A**. In these animals although surface CD19 is expressed from early pro-B cell stage/fraction B onwards **(supplementary data Fig. 4.1B**), only ~15% of this B cell subset was YFP$^+$ **(Fig. 3A)**. However, in these animals Cre expression increases at later stages of bone marrow development compared to *Mb1*-iCre/Rosa26-*YFP* strain(28) resulting in ~90% YFP labelling detectable in mature B/fraction F cells (**Fig. 3A**). In these mice, while YFP expression was found in ~90% of peritoneal B cells from *Cd19*-Cre/Rosa26-*YFP* mice, very small numbers of YFP$^+$ Mφs were found in this *Cd19*-Cre reporter strain; similar data were obtained using *Cr2*-Cre reporter mice where YFP expression is also restricted to mature B cell populations (**Fig. 3B**). These data along with those in **Fig. 2C** (no V-DJ re-arrangements detectable in YFP+ Mφs) suggest that YFP+ Mφs found in *Mb1*-iCre/Rosa26-*YFP* mice are not derived from mature B cells.

Next we investigated whether YFP$^+$ Mφs developed in *Mb1*-iCre/Rosa26-*YFP* mice that were also deficient in *Rag2* gene and therefore lacked mature B cells due to a developmental block at the bone marrow pro-B cell stage(29). The frequency of YFP$^+$ Mφs in the peritoneal cavity of *Rag2*$^{-/-}$*/Mb1*-iCre/Rosa26-*YFP* were similar to those detected in B cell-sufficient *Rag2*$^{+/+}$*/Mb1*-iCre/Rosa26-*YFP* mice (**Fig. 3B**). These data and those presented in **Fig. 2** suggest that tissue-resident YFP$^+$ Mφs are not derived from mature B cells, but arise from an immature B cell population with non-rearranged BCR genes, most likely within pro-B cells. As a proportion of early pro-B/fraction B cells have not undergone rearrangement(30), we suspect that it's this population that harbour novel precursors that are an alternative source of Mφs in adulthood.

In support of this hypothesis we found B220$^+$CD43$^+$ early B cells in bone marrow **(Fig. 4A)** as well as in blood **(Fig. 4B)** that were also CD19$^+$YFP$^+$CD16/32^{++}CD11b$^+$. High levels of CD16/32 and CD11b expression, which are commonly found on myeloid cell populations (**supplementary Fig. 4.2**), suggest that this population might be a potential precursor of YFP$^+$ Mφs. Indeed, back-gating analysis revealed that these cells are found within early pro-B/fraction B cells in the bone marrow

(**Fig. 4C**). The majority of these cells in bone marrow were also $Gr1^+$, while only ~30% expressed Gr1 in blood; both bone marrow and blood cell populations expressed very little, if any, IL7Rα (**supplementary Fig. 4.3B**).

Therefore, the absence of YFP^+ Mφs in *Cd19*-Cre/Rosa26-*YFP*, but their presence in *Rag2*$^{-/-}$*/Mb1*-iCre/Rosa26-*YFP* mice suggests that YFP^+ Mφs in *Mb1*- iCre/Rosa26-*YFP* mice might be derived from non-rearranged $B220^+CD43^+CD19^+YFP^+CD16/32^{++}CD11b^+$ cells within early pro-B/Fraction B cells. Consequently, YFP^+ Mφs are hereafter referred to as "pB-Mφs" for cells derived from a population within early pro B cells. In addition, $B220^+CD43^+CD19^+YFP^+CD16/32^{++}CD11b^+$ B cells that give rise to pB-Mφs are called "pB-$M\varphi^{precursors}$".

Pro-B cell-derived Mφs are generated in response to inflammation

To determine the dynamic relationship between pB-$M\varphi^{precursors}$ and pB-Mφs we injected zymosan(31) into the peritoneum of *Mb1*-iCre/Rosa26-*YFP* mice. Zymosan triggers an acute resolving inflammation causing immediate changes in cellular trafficking within the peritoneum as well as in blood and bone marrow. In the naïve peritoneum and shown previously in **Fig. 1B,** YFP^- embryonic-derived Mφs as well as YFP^+ pB-Mφs were identified within the $B220^-CD19^-$ fraction; however, both populations were also $CD16/32^{++}$. Within $B220^+CD19^+$ B cells a subset that co-expressed $CD16/32^{++}CD11b^{++}$ and YFP^+ was identified (**Fig. 5A)**. This latter population was phenotypically similar to pB-$M\varphi^{precursors}$ in bone marrow and blood (**Fig. 4A-B**). After 4h of zymosan injection $CD19^-YFP^-$ embryonic Mφs and pB-Mφs transiently disappeared from the peritoneum consistent with the "leukocyte disappearance phenomenon"(32) while numbers of peritoneal pB-$M\varphi^{precursors}$ increased at onset, but declined from 24 to 72h after zymosan injection (**Fig. 5B**); the temporal profiles of these cells are shown in **Fig. 5C**.

pB-$M\varphi^{precursors}$ detected within the B cell compartment at 4h underwent phenotypic changes over the course of inflammation by down-regulating expression of Gr1 and CD43, but up-regulating CD115, F4/80 and CD16/32 (**Fig. 5D**). As pB-$M\varphi^{precursors}$ differentiated into Mφs from 24h after zymosan administration they lost CD19 and B220 expression and acquired Mφ characteristics

including expression of F4/80 and higher levels of CD11b and CD16/32 coincident with the increase in the numbers of pB-Mφs from 24h onwards, **Fig. 5D**.

Consistent with the idea that biphenotypic cells within bone marrow pro-B/Fraction B gives rise to YFP^+ Mφ, the proportion of pB-$M\varphi^{precursors}$ in bone marrow increased at 4h post-peritonitis and gradually returned to pre-inflammation levels by 72h (**Fig. 5D**). Changes in peripheral blood pB-$M\varphi^{precursors}$ correlated inversely with the fluctuations in bone marrow pB-$M\varphi^{precursors}$ demonstrating a transient decrease at inflammatory onset and recovery by resolution (**Fig. 5E**). These data, taken together with an increase in peritoneal pB-$M\varphi^{precursors}$ during the early stage of inflammation (**Fig. 5C**) reflect the generation and expansion of bone marrow pB-$M\varphi^{precursors}$ triggered by inflammation followed by their migration *via* the blood stream into the peritoneum and their further differentiation into inflammatory pB-Mφ.

We next tested the potential of pB-$M\varphi^{precursors}$ to proliferate in either myeloid or lymphoid cocktails over 14 days in culture. Using CMPs and proB cells as controls, pB-$M\varphi^{precursors}$ grow only in a myeloid cocktail and did not respond to growth factors that support lymphocyte growth, **Fig 6A**; this is consistent with virtually undetectable levels of IL7Ra on these cells, **Supplementary Fig. 4.3C**. We also tested the ability of FACS-purified peritoneal pB-$M\varphi^{precursors}$ to differentiate into Mφs *in vitro*. We used pB-$M\varphi^{precursors}$ collected at 4h post-peritonitis as they were quantitatively enriched during that phase when compared to the naïve peritoneum; naïve peritoneal B cells ($CD19^+Gr1^-CD11b^{+/-}F4/80^-$) were used as control. After 6 days of cultivation in presence of M-CSF small and distinctively round pB-$M\varphi^{precursors}$ differentiated into cells with characteristic Mφ morphology as they increased their cell size and acquired F4/80 expression (**Fig. 6B-C**). Significantly fewer cells acquired these Mφ characteristics when cultivated in the absence of M-CSF or presence of GM-CSF (**Fig. 6C and for further comparisons see Supplementary Fig. 5.1**).

Early pro-B cells reconstitute tissue Mφs *in vivo* following lethal irradiation

FACS-purified bone marrow YFP^+ early pro-B/fraction B cells comprising biphenotypic $CD19^+B220^+YFP^+CD16/32^{++}CD11b^+$ pB-$M\varphi^{precursors}$ (**Fig. 4A** and **supplementary Fig. 6.1**) were

injected into lethally irradiated wild type mice along with CD45.1^{+} total bone marrow from congenic wild type mice to improve survival rates following irradiation. Mature bone marrow B cell/fraction F subset (**supplementary Fig. 6.1**) in combination with CD45.1^{+} total bone marrow was used as a control. Data in **Fig. 7A** depicts B cell and Mφ composition of the peritoneum of naïve wild type CD45.1 mice alongside Mb-1iCre/Rosa26-YFP mice, which are on a CD45.2 background. Adoptive transfer of CD45.1^{+} bone marrow resulted in reconstitution of all lineages, while early pro-B cells contributed to the restoration of B cell lineage in the peritoneum **(Fig. 7B)** and spleen (**Fig. 7C**). Importantly, adoptively transferred biphenotypic pB-Mφ^{precursors} within early pro-B cells gave rise to YFP^{+} Mφs in the peritoneum, but did not contribute to myeloid populations in the spleen (**Fig. 7C** and **supplementary Fig. 6.2 B and C**). While YFP expression was found in roughly 7% of CLPs **(supplementary Fig. 1.2B)** there was no YFP^{+} mature T cells found in the spleens of recipient mice (**Fig. 7C**); moreover, transfer of Lin^{-}IL7Rα^{+}Sca-1^{++}c-Kit^{++} CLPs containing YFP^{+} CLPs to lethally irradiated mice did not result in the appearance of YFP^{+} Mφs in these animals (**Fig. 7D**). Also, upon the transfer of Mb-1iCre/Rosa26-YFP LMPPs into sublethally-irradiated CD45.1+ Rag2-null recipients no evidence of the reporter was found in the hosts (Table S1), consistent with 0% YFP reporter expression in these cells, **Supplementary Fig. 1.2B.** These findings provide evidence that early pro-B cells and specifically biphenotypic pB-Mφ^{precursors} and not mature B cells or contaminating CLPs differentiate into Mφs *in vivo*.

Transcriptomic analysis of pro-B cell-derived Mφs and their 'classical' counterparts

In the first instance, it was necessary to discriminate between Mφ populations present in the naïve peritoneum and those that appear during inflammatory resolution. To do this we used the phagocytic dye PKH26PCL (PKH-Red), which labels resident peritoneal phagocytes(33) but not infiltrating pB-Mφ^{precursors} or peripheral blood monocytes (**supplementary Fig. 7.1**). Embryonically derived Mφs and pB-Mφs were further designated as Mφs$^{TR\text{-}naïve}$ (P1) and pB-Mφs$^{TR\text{-}naïve}$ (P2), respectively, to highlight they are ***T***issue ***R***esident cells from the ***naïve*** peritoneum. Injecting PKH-Red into Mb1-iCre/Rosa26-YFP mice prior to inflammation resulting Mφs$^{TR\text{-}naïve}$ and pB-Mφs$^{TR\text{-}naïve}$ becoming PKH-PCL positive. Injecting zymosan shortly after PKH-PCL and examining the cavity

during resolution revealed four additional inflammatory Mφ populations including Mφs$^{TR\text{-}naïve}$ that experienced 72h of inflammation and are hereafter called Mφs$^{TR\text{-}inflam}$ (P3) and monocyte-derived mo-Mφs^{inflam} (P4) as they are YFP^{-}PKH^{-}. In addition, pB-Mφs$^{TR\text{-}naïve}$ that experienced 72h of inflammation were detected and named pB-Mφs$^{TR\text{-}inflam}$ (P5) while pB-Mφ^{precursors} that infiltrated into the cavity in response to zymosan (evident at 4h in **Fig. 5B**) and that also experienced 72h of inflammation were detected and designated pB-Mφs^{inflam} (P6), **Fig. 8A**.

Gene expression profiles for these naïve and inflammation-experienced Mφ populations were then analysed, see Methods section for microarray and sample preparation as well as **supplementary Figs. 7.2-7.3** for gating strategies. First, we compared global gene expression profiles of individual cell populations (30 datasets, n=3 per group) by performing a sample-to-sample correlation analysis using the Biolayout Express3D software tool(34) with a Pearson correlation threshold of r ≥ 0.97. This analysis showed that monocytes, neutrophils, B-1 and B-2 B cells data sets (these additional cells types were included for comparison purposes) clustered together like-with-like in distinct regions of the graph, while all Mφ populations formed a single, distinct component within this network (**Fig. 8B)**. Within this component, naïve tissue-resident pB-Mφ$^{TR\text{-}naïve}$ and Mφ$^{TR\text{-}naïve}$ were located like-with-like as were inflammatory tissue-resident pB-Mφ$^{TR\text{-}inflam}$ and Mφ$^{TR\text{-}inflam}$ as well as inflammation-induced pB-Mφ^{inflam} and mo-Mφ^{inflam}. These data suggest that pB-Mφs and 'classical' Mφs that are embryonically derived share highly similar overall transcriptional profiles. Network correlation and cluster analysis of transcript co-expression shown in **Fig. 8C** revealed gene clusters with similar functions or cell-specific activities occupying specific cliques within the network graph. **Table S2** provides the contents of each of these clusters, and the expression profiles of selected clusters across the 30 data sets are displayed in **supplementary data Fig. 7.5 A-D** and **supplementary Fig. 7.4**. For example, cluster C2 and C4 contained many genes expressed highly by B cells (**supplementary data Fig. 7.5A**) including *Cd19* and many immunoglobulin-encoding genes including *IgH-V11* **supplementary data Fig. 7.5B**). Clusters C5, C17, and C50 were enriched with genes known to be expressed highly by Mφs(35) (**supplementary data Fig. 7.5C**). Genes within these clusters were expressed highly by all monocyte and Mφ populations represented in this analysis, when compared to B cells and

neutrophils (**Fig. 6G**). In contrast, only very low levels of genes within the B cell-related clusters were detected in any of the Mφ data sets including those derived from pro-B cells (**supplementary data Fig. 7.5A-C**), and their expression levels were consistent with our post-sort purity analysis data, which indicated the presence of low levels of contaminating B cells (0-10%) in some Mφ samples (**Supplementary Fig. 7.2**). Importantly genes in clusters C55 and C71 were expressed highly by both types of inflammation-induced Mφs including pB-Mφ^{inflam} as well as mo-Mφ^{inflam} in comparison to other Mφs populations (**Fig. Supplementary 7.4F**), while embryonic and pro-B cell-derived Mφs from naïve peritoneum (Mφ$^{TR\text{-}naïve}$ and pB-Mφ$^{TR\text{-}naïve}$) and following inflammation (Mφ$^{TR\text{-}inflam}$ and pB-Mφ$^{TR\text{-}inflam}$) characteristically expressed genes included in clusters C6, C36 and C40 (**Supplementary 7.4G**). Hence transcriptome analysis also reveals the plasticity of the pro-B-derived Mφ precursors that give rise to two distinct subsets of Mφs with vastly contrasting phenotypes during homeostasis (pB-Mφ$^{TR\text{-}naïve}$) and inflammation (pB-Mφ^{inflam}). Genes in all of the mononuclear phagocyte-related clusters were expressed highly in pB-Mφs at similar levels to those expressed by embryonic/monocyte-derived Mφs counterparts. No clusters were identified which contained unique genes expressed highly in pB-Mφs alone. Similarly, no genes were identified, which were expressed highly in embryonic/monocyte-derived Mφs, but not in pB-Mφs. Together these data suggest that despite the distinct origin of the pro-B cell-derived Mφs, they share very similar transcriptional and therefore predicted phenotypic characteristics with ‘classical’ Mφ populations, i.e. embryonic/monocyte-derived Mφs.

DISCUSSION

Our study highlights the developmental plasticity of immature B cells and their role as an additional source of Mφs *in vivo*. Here we provide evidence of a subset of early pro-B cells with non-rearranged BCR that differentiate into Mφs during homeostasis and inflammation. In this work we used a combination of B cell-specific reporter mice including *Mb1*-iCre/Rosa26-*YFP*, *Cd19*-Cre/Rosa26-*YFP*, and *Rag2*$^{-/-}$*/Mb1*-iCre/Rosa26-*YFP*, which enabled fate mapping studies to establish that a proportion of tissue-resident Mφs in serous cavities and intestine are derived from a novel sub-population of non-rearranged early pro-B cells co-expressing B cell and myeloid markers.

These findings are fundamentally distinct from earlier reports, which demonstrated myeloid lineage switch occurring in early lymphoid progenitors *in vitro*(12, 36, 37) as well as B cell-to-Mφ differentiation using enforced C/EBPα expression(15, 16, 38). Indeed, bi-potential progenitors that give rise to Mφs have been reported in postnatal bone marrow(39). However, these cells are different to pB-Mφ^{precursors} reported here, as they are CD45R^{-}CD19^{+}CD127^{+}CD11b^{-}Gr1^{-} and D-J^{+}. Moreover, AA4.1^{+}B200^{-}Mac1^{-}Ly6A^{+} bi-potential progenitors in foetal liver(12) and adult bone marrow early progenitors with lymphoid and myeloid potential (EPLMs) expressing B220, c-Kit, IL-7Rα (CD127), Flt3 (CD135) and CD93, but not CD19 and NK1.1(10), demonstrate both lymphoid and myeloid potential *in vitro*. While the above reports and other studies used primarily artificial experimental systems(17-19) we demonstrate a novel bi-phenotypic population within early pro-B cell that contributes significantly to Mφs populations *in vivo*, representing a normal facet of haematopoiesis.

Although YFP expression was detected in some CLPs, very few mature T cells (<0.5%) and indeed thymic progenitors (~0.15%) expressed YFP. We suspect that the vast majority of YFP^{+} CLPs (Lin^{-}IL7Rα^{+}Sca-1^{+}c-Kit^{+}) are committed toward a B cell differentiation pathway as YFP expression within these CLPs is enabled by *Cd79a (Mb-1)* promoter activation driven, in turn, by E2A and EBF transcription factors, which initiate early B cell lymphopoiesis(40). Indeed, the complete absence of eYFP expression on mature myeloid cells after transfer of Mb-1iCre/Rosa26-

YFP LMPPs into alympoid recipients would strongly argue that in the generation of graft-derived myeloid cells in this model does not originate from a LMPP progenitor. Therefore, these progenitors are unlikely to account for selective YFP expression in tissue-resident Mφ populations in the peritoneum, pleural cavity and intestine. This assertion is reinforced by the lack of YFP^+ Mφs in irradiated mice receiving YFP^+ CLPs.

The molecular signals that enable a myeloid fate in the subset of early pro-B cells described here remains to be elucidated. However, it's likely that the demand for Mφs in tissues generates these signals. Indeed, this became evident during zymosan-induced peritonitis where local inflammatory factors triggered the expansion of bone marrow pB-$M\varphi^{precursors}$, which egressed into blood and accumulated in the peritoneum where they differentiated into inflammatory pro-B cell-derived Mφs (pB-$M\varphi^{inflam}$). While these temporal changes are certainly only correlative, these data suggest that not only do bone marrow pB-$M\varphi^{precursors}$ seed the peritoneal and pleural cavity as well as the gastrointestinal system during homeostasis, but that these circulating blood precursors enter the sites of infection/injury and generate Mφ during inflammation. Notably, despite their different origins, pB-Mφs are transcriptomically similar to embryonic Mφs during steady state/homeostasis, but are phenotypically distinct from those generated by pB-$M\varphi^{precursors}$ during inflammation thereby emphasizes the functional plasticity of pB-$M\varphi^{precursors}$, which is likely to be determined by the tissue environment and inflammatory signals they receive.

Consistent with the lack of IL7 receptor on pB-$M\varphi^{precursors}$, *in vitro* assays revealed the propensity of these cells to differentiate down a myeloid lineage. Indeed, reconstitution of tissue-resident Mφs in lethally irradiated mice was observed by adoptively transferring these early pro-B cells, but not LMPPs or CLPs. In terms of the origin of these cells, bone marrow pB-$M\varphi^{precursors}$ as well as the $CD19^+YFP^+V\text{-}DJ^-$ intermediate Mφs in the peritoneum express CD19 as extensively verified by a number of methods including single cell profiling. CD19 expression on the cells, which is strictly controlled by the transcription factor PAX5, suggests their close developmental relationship with B cells (41). ~~*These data indicate a hematopoietic progenitor present within bone marrow Fraction B that evidence Mφs development potentials and co-express certain markers of both lymphoid and*~~

~~*myeloid lineages.*~~ It must be emphasized that these precursors lack detectable immunoglobulin rearrangements and they are unable to generate B lineage cells in B cell-promoting culture conditions. In which case, its likely that these bi-phenotypic macrophage precursors are committed to the myeloid lineage but express transiently some B lineage markers. We believe, that this mechanism is an additional source of tissue Mφs and is an intrinsic part of normal haematopoiesis *in vivo*. In summary, the discovery of novel Mφ subsets arising from pro-B cells reveals an alternative source of Mφs during homeostasis and inflammation. These data significantly advance and expand our understanding of Mφ biology and haematopoiesis, the plasticity of hematopoietic precursors and the heterogeneity of Mϕ subsets.

MATERIALS AND METHODS

Animals

C57BL/6 (Harlan), *B6.129P2-Cd19<tm1(cre)Cgn/J, B6.Cg-Tg(Cr2-cre)3Cgn/J* (Jackson Laboratories), Rosa26-*YFP* (kindly provided by Ulla Dennehy, London, UK), B6.CD45.1 (kindly provided by Prof B. Stockinger, London, UK) and B6.*Mb1*-iCre (kindly provided by Prof M. Reth, Freiburg, Germany) mice (male 6-8 weeks old) were housed and breed in pathogen free conditions. All experiments were performed in compliance with United Kingdom Home Office regulations.

Peritonitis and resident phagocytic cell labelling

Self-resolving peritonitis was induced by intraperitoneal (i.p) injection of sterile zymosan A, from *Saccharamyces cerevisiae* (Sigma) solution in PBS at a dose of 0.1 mg/mouse. Peritoneal cells were collected from naïve animals and 4, 16/24, 48 and 72h post-inflammation. For labelling of resident peritoneal phagocytes 0.5 ml of 0.5 μM PKH26PCL (PKH-Red) fluorescent cell linker (Sigma) solution in diluent B (Sigma) was injected IP prior induction of peritonitis accordingly to manufacturer's instructions.

Bone marrow adoptive transfer/

C57BL/6 mice (CD45.2) were lethally irradiated with single dose of 950 RAD and reconstituted with $2.5x10^6$ donor bone marrow cells. Each mouse received i.v. injection of mixed population of FACS-purified YFP^+ bone marrow B cells from *Mb1*-iCre/Rosa26-*YFP* mice and total $CD45.1^+$ bone marrow cells from congenic wild-type strain at 1:10 ratio. Total early pro-B cells ($YFP^+B220^+CD19^+CD43^+CD24^+BP\text{-}1^-$) containing biphenotypic $YFP^+CD16/32^{++}CD11b^{++}$ pB-$M\varphi^{precursors}$ or mature bone marrow B cells ($YFP^+B220^{high}CD19^+CD43^-CD24^{low}$) were analysed for their potential to reconstitute tissue Mφs, while $CD45.1^+$ total bone marrow cells were injected into animals to improve the survival rates following lethal irradiation. Haematopoietic reconstitution was analysed by flow cytometry analysis in peritoneum and spleen at 2, 4 and 6 weeks following irradiation and adoptive transfer.

Flow cytometry and cell sorting

Flow cytometry and cell sorting were performed on LSR-II/LSR-Fortessa and FACSAria (BD Biosciences), respectively. For flow cytometry analysis 0.5-1x10^6 of freshly isolated cells reconstituted in FACS buffer and incubated with Fc-Blocker (AbD Serotec) were stained in final volume of 50 µl for 20-30 min and then washed 3 times with 150 µl of FACS buffer. For FACS sorting cells were re-suspended at 10x10^6 cells /40 µl of FACS buffer. Following antibodies were used: CD11b-PerCP-Cy5.5/V450/Alexa-700, CD19-Alexa Fluor 700/PE, CD23-PE-Cy7, CD21-APC, IgM-PE/PE-Cy7/Biotin, Gr1-APC/PE, B220-Alexa-700/Horizon-V500, BP-1(Ly-51)-Biotin, CD24(HSA)-PE-Cy7, Streptavidin-APC/Horizon-V450/Horizon-V500 from BD Pharmingen; CD19-FITC, B220-RPE, F4/80-APC from AbD Serotec; MHC-II-PE/FITC/Alexa-700, F4/80-APC/PE-Cy7/PerCP-Cy5.5, CD115-PE/APC, CD16/32(FcγR)-PerCP-Cy5.5, CD34-Alexa Fluor 700 and CD127(IL7Ra)-PE-Cy7 from eBioscience; biotyinilated Abs for lineage markers were purchased from eBiosciences: CD3(17A2), CD4(GK1.5), CD8(53-6.7), CD19(1D3), B220(RA3-6B2), IgM(R6-60.2), Gr1(RB6-8C5), CD11b(M1/70), Ter119(TER119), NK1.1.(PK136); Live/Dead viability dye from Invitrogen. Flow cytometry data analysis was performed with FlowJo vX.0.7 software (Tree Star) using fluorescence minus one control samples as reference for setting gates.

Statistical analysis

Statistical evaluation of data was performed in GraphPad Prism (GraphPad Software) by an unpaired *t*-test in case of two groups and one-way ANOVA using Bonferroni post-test. A P-value of less than 0.05 was considered statistically significant (*P < 0.05, **P < 0.01, ***P < 0.001). Statistical analysis of BCR sequencing and microarray data was performed using R project software.

For BCR re-arrangements assessment, detection of B cell- and Mφ-specific mRNA transcripts were amplified by RT-PCR, Microarray analysis and Hematopoietic cell isolation please see Supplementary materials and methods.

ACKNOWLEDGMENTS

The work carried out in this report was sponsored by the Wellcome Trust in the form of a Senior Research Fellowship to Prof Derek W Gilroy, and Institute Strategic Programme Grant funding from the Biotechnology and Biological Sciences Research Council to Prof. Neil Mabbbott and Prof. Tom Freeman. The authors wish to acknowledge Dr Brigitta Stockinger from the National Institute for Medical Research, Mill Hill, UK for supply off *Rag2*$^{-/-}$ mice. We also wish to thank Dr Michael Reth, Max Plank Institute of Immunobiology and Epigenetics for supplying *Mb-1*iCre mice and Ulla Dennehy from University College London, UK for supplying Rosa26-YFP mice. Thanks to Dr. Edward Tsao for advice and training on RNA preparation.

ACCESSION NUMBERS

Microarray data are archived under ArrayExpress accession number E-MTAB-1878.

SUPPLEMENTAL INFORMATION

Supplemental Figures S1-S7 and supplemental Tables S1 and S2.

AUTHOR CONTRIBUTION

DWG and TA devised experiments and wrote the paper. RBR and PK provided invaluable help and direction with designing of primers and single cell PCR. AP provided data on analysis of bone marrow precursors as well as transfer of cells into Rag mice. DF carried out statistical analysis on transcriptomic data while TF and NM were responsible for array data bioinformatics analysis and presentation.

CONFLICT OF INTEREST

RBR is a Consultant for VHSquared while all other authors declare no conflict of interest.

REFERENCES

1. Ginhoux F & Jung S (2014) Monocytes and macrophages: developmental pathways and tissue homeostasis. *Nat Rev Immunol* 14(6):392-404.
2. Gordon S & Taylor PR (2005) Monocyte and macrophage heterogeneity. *Nat Rev Immunol* 5(12):953-964.
3. Bain CC*, et al.* (2013) Resident and pro-inflammatory macrophages in the colon represent alternative context-dependent fates of the same Ly6Chi monocyte precursors. *Mucosal Immunol* 6(3):498-510.
4. Hoeffel G*, et al.* (2015) C-myb(+) erythro-myeloid progenitor-derived fetal monocytes give rise to adult tissue-resident macrophages. *Immunity* 42(4):665-678.
5. Gomez Perdiguero E*, et al.* (2015) Tissue-resident macrophages originate from yolk-sac-derived erythro-myeloid progenitors. *Nature* 518(7540):547-551.
6. Rosas M*, et al.* (2014) The transcription factor Gata6 links tissue macrophage phenotype and proliferative renewal. *Science* 344(6184):645-648.
7. Okabe Y & Medzhitov R (2014) Tissue-specific signals control reversible program of localization and functional polarization of macrophages. *Cell* 157(4):832-844.
8. Schulz C*, et al.* (2012) A lineage of myeloid cells independent of Myb and hematopoietic stem cells. *Science* 336(6077):86-90.
9. Ginhoux F*, et al.* (2010) Fate mapping analysis reveals that adult microglia derive from primitive macrophages. *Science* 330(6005):841-845.
10. Ceredig R, Rolink AG, & Brown G (2009) Models of haematopoiesis: seeing the wood for the trees. *Nat Rev Immunol* 9(4):293-300.
11. Kawamoto H & Katsura Y (2009) A new paradigm for hematopoietic cell lineages: revision of the classical concept of the myeloid-lymphoid dichotomy. *Trends Immunol* 30(5):193-200.
12. Cumano A, Paige CJ, Iscove NN, & Brady G (1992) Bipotential precursors of B cells and macrophages in murine fetal liver. *Nature* 356(6370):612-615.
13. Wada H*, et al.* (2008) Adult T-cell progenitors retain myeloid potential. *Nature* 452(7188):768-772.

14. Adolfsson J*, et al.* (2005) Identification of Flt3+ lympho-myeloid stem cells lacking erythro-megakaryocytic potential a revised road map for adult blood lineage commitment. *Cell* 121(2):295-306.

15. Heavey B, Charalambous C, Cobaleda C, & Busslinger M (2003) Myeloid lineage switch of Pax5 mutant but not wild-type B cell progenitors by C/EBPalpha and GATA factors. *Embo J* 22(15):3887-3897.

16. Xie H, Ye M, Feng R, & Graf T (2004) Stepwise reprogramming of B cells into macrophages. *Cell* 117(5):663-676.

17. Almeida SR*, et al.* (2001) Mouse B-1 cell-derived mononuclear phagocyte, a novel cellular component of acute non-specific inflammatory exudate. *Int Immunol* 13(9):1193-1201.

18. Popi AF*, et al.* (2009) Co-ordinated expression of lymphoid and myeloid specific transcription factors during B-1b cell differentiation into mononuclear phagocytes in vitro. *Immunology* 126(1):114-122.

19. Popi AF, Osugui L, Perez KR, Longo-Maugeri IM, & Mariano M (2012) Could a B-1 Cell Derived Phagocyte "Be One" of the Peritoneal Macrophages during LPS-Driven Inflammation? *Plos One* 7(3).

20. Hobeika E*, et al.* (2006) Testing gene function early in the B cell lineage in mb1-cre mice. *Proc Natl Acad Sci U S A* 103(37):13789-13794.

21. Srinivas S*, et al.* (2001) Cre reporter strains produced by targeted insertion of EYFP and ECFP into the ROSA26 locus. *BMC Dev Biol* 1:4.

22. Hardy RR, Carmack CE, Shinton SA, Kemp JD, & Hayakawa K (1991) Resolution and characterization of pro-B and pre-pro-B cell stages in normal mouse bone marrow. *The Journal of experimental medicine* 173(5):1213-1225.

23. Hardy RR & Hayakawa K (2001) B cell development pathways. *Annu Rev Immunol* 19:595-621.

24. Rolink A & Melchers F (1991) Molecular and cellular origins of B lymphocyte diversity. *Cell* 66(6):1081-1094.

25. Borrello MA & Phipps RP (1999) Fibroblast-secreted macrophage colony-stimulating factor is responsible for generation of biphenotypic B/macrophage cells from a subset of mouse B lymphocytes. *J Immunol* 163(7):3605-3611.

26. Borrello MA, Palis J, & Phipps RP (2001) The relationship of CD5+ B lymphocytes to macrophages: insights from normal biphenotypic B/macrophage cells. *Int Rev Immunol* 20(1):137-155.

27. Takahashi K*, et al.* (1998) Effects of granulocyte/macrophage colony-stimulating factor on the development and differentiation of CD5-positive macrophages and their potential derivation from a CD5-positive B-cell lineage in mice. *Am J Pathol* 152(2):445-456.

28. Rickert RC, Roes J, & Rajewsky K (1997) B lymphocyte-specific, Cre-mediated mutagenesis in mice. *Nucleic Acids Res* 25(6):1317-1318.

29. Shinkai Y*, et al.* (1992) RAG-2-deficient mice lack mature lymphocytes owing to inability to initiate V(D)J rearrangement. *Cell* 68(5):855-867.

30. Hardy RR, Carmack CE, Shinton SA, Kemp JD, & Hayakawa K (2012) Resolution and characterization of pro-B and pre-pro-B cell stages in normal mouse bone marrow. 1991. *J Immunol* 189(7):3271-3283.

31. Stables MJ*, et al.* (2011) Transcriptomic analyses of murine resolution-phase macrophages. *Blood* 118(26):E192-E208.

32. Sultan AM, Dunn CJ, Mimms PC, Giroud JP, & Willoughby DA (1978) The leucocoyte disappearance reaction in non-immune acute inflammation. *J Pathol* 126(4):221-230.

33. Melnicoff MJ, Morahan PS, Jensen BD, Breslin EW, & Horan PK (1988) In vivo labeling of resident peritoneal macrophages. *J Leukoc Biol* 43(5):387-397.

34. Freeman TC*, et al.* (2007) Construction, visualisation, and clustering of transcription networks from microarray expression data. *PLoS computational biology* 3(10):2032-2042.

35. Hume DA, Summers KM, Raza S, Baillie JK, & Freeman TC (2010) Functional clustering and lineage markers: insights into cellular differentiation and gene function from large-scale microarray studies of purified primary cell populations. *Genomics* 95(6):328-338.

36. Mikkola I, Heavey B, Horcher M, & Busslinger M (2002) Reversion of B cell commitment upon loss of Pax5 expression. *Science* 297(5578):110-113.

37. Reynaud D, Lefort N, Manie E, Coulombel L, & Levy Y (2003) In vitro identification of human pro-B cells that give rise to macrophages, natural killer cells, and T cells. *Blood* 101(11):4313-4321.

38. Bussmann LH*, et al.* (2009) A robust and highly efficient immune cell reprogramming system. *Cell Stem Cell* 5(5):554-566.

39. Montecino-Rodriguez E, Leathers H, & Dorshkind K (2001) Bipotential B-macrophage progenitors are present in adult bone marrow. *Nat Immunol* 2(1):83-88.

40. Busslinger M, Nutt SL, & Rolink AG (2000) Lineage commitment in lymphopoiesis. *Curr Opin Immunol* 12(2):151-158.

41. Nutt SL, Urbanek P, Rolink A, & Busslinger M (1997) Essential functions of Pax5 (BSAP) in pro-B cell development: difference between fetal and adult B lymphopoiesis and reduced V-to-DJ recombination at the IgH locus. *Genes Dev* 11(4):476-491.

Figure 1. Mφs with a potential B cell origin detected in *Mb1*-iCre/Rosa26R-*YFP* reporter mice. a, Flow cytometric analysis of wild type C57BL6 mice showing CD19 expression on peritoneal $CD11b^{++}F4/80^{++}$ Mφs. **(b)** Equivalent analysis of *Mb1*-iCre/Rosa26-*YFP* mice showing YFP expression pattern in Mφs from various tissues. Representative data shown for n=10 experiments carried out on naïve animals.

Figure 2. YFP^+ Mφs in *Mb1*-iCre/Rosa26R-*YFP* mice do not arise form mature B cells. a, ImageStream analysis of nave murine peritoneum. Dot-plots showing single focused cells in $CD11b^{++}F4/80^{++}$ Mφ gate identifying 3 Mφ populations: $CD19^-YFP^-$, $CD19^-YFP^+$ and $CD19^+YFP^+$; non-Mφ ($CD11b^{+/-}F4/80^-$) compartment containing $CD19^+YFP^+$ B cells. **b,** Representative images of $CD11b^{++}F4/80^{++}$ Mφ populations and B cells are shown. While confirming the presence of Mφs co-expressing CD11b, F4/80, YFP and CD19, ImageStream reveals a substantial amount of doublets occur within rare population of $CD19^+YFP^+$ Mφs; the frequency of single bi-phenotypic cells within $CD19^+YFP^+$ Mφ gate constitute ~16.74 % (see table). **c,** Detection of V-DJ re-arrangements and expression B cell- and Mφ-specific genes in single and multiple cells purified by FACS. At least 45 single and multiple (20/10/5) cells of each type, including peritoneal B-1/B-2 B cells, and $CD11b^{++}F4/80^{++}$ Mφ populations: $CD19^-YFP^-$, $CD19^-YFP^+$ and $CD19^+YFP^+$, were analysed for presence of V-DJ re-arrangements in genomic DNA, B cell-specific *Cd79b* transcript and Mφ-specific *Emr1* transcript. The frequency of $V\text{-}DJ^+$ reactions shown at the bottom of the graph demonstrating that despite co-expression of *Cd79b* and *Emr1* in intermediate $CD19^+YFP^+$ Mφs low number (15 out of 45 versus 32 out of 45) of $V\text{-}DJ^+$ reactions compared to B cells is detected on single cell level. The number of $V\text{-}DJ^+$ reactions increase (38 out of 45) to B cell levels, when multiple cells (20/10/5) of $CD19^+YFP^+$ Mφs are analysed per reaction, suggesting contamination by B cells.

Figure 3. Evaluation of B cell-specific reporter mice point toward early pro-B cell origin of YFP^+ Mφs. Cells and tissues from *Mb1*-iCre/Rosa26-*YFP* mice (*Mb1*-iCre), *CD19*-Cre/Rosa26-*YFP* mice (*CD19-Cre*), *Rag2*$^{-/-}$*/Mb1*-iCre/Rosa26-*YFP* mice (*Rag2*$^{-/-}$*/ Mb1*-iCre), *Cr2*-Cre/Rosa26-*YFP* mice (*Cr2*-Cre) and Rosa26-*YFP* mice were collected and analysed by flow cytometry. **a,** Representative dot-plots showing induction of YFP expression at later B cell bone marrow

developmental stages in *CD19*-Cre/Rosa26-*YFP* mice (*CD19-Cre*) as compared to *Mb1*-iCre/Rosa26-*YFP* mice (*Mb1*-iCre). For gating strategy see **Supplementary Fig. 4.1a & b,** Representative dot-plots showing YFP expression in peritoneal $CD19^{+}$ B cells and $CD11b^{++}F4/80^{++}$ Mφs in mouse strains above.

Figure 4. Bi-phenotypic populations of $CD19^{+}B220^{+}CD43^{+}YFP^{+}CD16/32^{++}CD11b^{+}$ with B-lymphoid and myeloid characteristics identified in bone marrow **(a)** and blood **(b)**. These cells will be further referred to as pB-$M\varphi^{precursors}$. **c**, Quantification of $CD19^{+}B220^{+}CD43^{+}YFP^{+}CD16/32^{++}CD11b^{+}$ pB-$M\varphi^{precursors}$ in early B cell bone marrow fractions. Values expressed in absolute numbers of cells per one limb.

Figure 5. YFP^{+} Mφs are generated from bi-phenotypic $B220^{+}CD43^{+}CD19^{+}$ $YFP^{+}CD16/32^{++}$ $CD11b^{+}$ pro-B cell-derived precursors in response to inflammation. Inflammation was induced by intraperitoneal injection of 0.1 mg zymosan. Tissues were collected at various time-points post peritonitis induction and anlysed by flow cytometry. **a**, Gating strategy showing identification of $B220^{+-}CD19^{+}$ B cells, $B220^{+-}CD19^{+}CD16/32^{++}CD11b^{++}$ peritoneal pB-$M\varphi^{precursors}$, $YFP^{-}B220^{-}CD19^{-}F4/80^{++}CD16/32^{++}CD11b^{++}$ Mφs and $YFP^{+}B220^{-}CD19^{-}F4/80^{++}CD16/32^{++}CD11b^{++}$ pB-Mφs in naïve peritoneum. **b**, Dot plots showing $B220^{+-}CD19^{+}$ B peritoneal compartment with increased proportion of $CD16/32^{++}CD11b^{++}$ pB-$M\varphi^{precursors}$ and $B220^{-}CD19^{-}$ compartment with reduced frequency of $F4/80^{++}CD11b^{++}$ Mφs at 4 hours post peritonitis induction. **c**, Temporal profiles of peritoneal Mφs, pB-Mφs and peritoneal pB-$M\varphi^{precursors}$ during inflammation with **d** showing cell surface markers for the cells over time. Panels **e** and **f** show the temporal profiles of pB-$M\varphi^{precursors}$ in bone marrow and peripheral blood, respectively, during inflammation. Values expressed as proportion form total bone marrow or blood cells. Statistical evaluation was performed by one-way ANOVA using Bonferroni post-test (*$P < 0.05$, **$P < 0.01$, ***$P < 0.001$).

Figure 6. In vitro assays for pro-B cell-derived precursors differentiation. (a) shows results of *in vitro* assay where single cell populations were cultured for 10-14 days in media supporting either myeloid or lymphoid growth with results shown as numbers of events bearing either lymphoid or myeloid phenotype in respective media as per materials/methods. **b,** FACS-purified peritoneal Mφs, B cells and pB-Mφ ^{precursors} from 4 hour peritonitis were cultured with/without M-CSF/GM-CSF and analysed by cell morphology using Rapid-Romanowsky stain and α-CD19, α-F4/80 and DAPI labelling. Scale bars, 20 μm. h, Cell size was quantified using ImageJ. Statistical evaluation was performed by one-way ANOVA using Bonferroni post-test (*P < 0.05, **P < 0.01, ***P < 0.001). ND = not detected.

Figure 7. pB-Mφ^{precursors} within early pro-B cell bone marrow fraction reconstitute peritoneal Mφs in lethally irradiated mice. FACS-purified early pro-B cells containing YFP+CD16/32++CD11b bi-phenotypic pB-Mφ^{precursors} and mature B cells (control) from bone marrow of *Mb1*- iCre/Rosa26-*YFP* mice **(see supplementary Fig. 6.1)** were mixed in ratio 1:10 with total bone marrow cells from congenic CD45.1 donor mice and injected i.v. into lethally irradiated (950 RAD) wild type mice. Haematopoietic reconstitution was assessed in peritoneum and spleen at 6 weeks post injection of donor bone marrow cells. **a** Representative plots showing tracing markers expression on peritoneal cell populations of naïve CD45.1 and *Mb1*-iCre/Rosa26-*YFP* mice and **b** engraftment of donor CD45.1+ (all lineages) and YFP+ (early pro-B/mature B) cells in peritoneum of lethally irradiated mice. **c** Haematopoietic lineages reconstitution analysis in spleen showing engraftment of CD45.1+ progenitors in B, T and myeloid compartment, while YFP+ early pro-B cells exclusively contribute to reconstitution of B cell lineage and do not differentiate into myeloid or T cells. **d** $Lin^{-}IL7R\alpha^{+}Sca\text{-}1^{++}c\text{-}Kit^{++}$ CLPs containing YFP^{+} CLPs was mixed with total bone marrow cells from congenic CD45.1 donor mice and injected into irradiated wild type mice and engraftment determined in the peritoneal B cell and myeloid compartments as well as spleen.

Figure 8. Pro-B cell-derived Mφs possess transcriptome profile similar to their embryonic and monocyte-derived counterparts. **a,** Inflammation was induced in *Mb-1*.iCre/Rosa26-*YFP* mice by intraperitoneal injection of 0.1 mg zymosan. Flow cytometry revealing (P1) YFP^- embryonic $M\varphi s^{TR\text{-}naive}$ and (P2) YFP^+ pro-B cell-derived pB-$M\varphi s^{TR\text{-}naïve}$ in naïve peritoneum. PHK-Red injected prior to peritonitis labels resident phagocytes and reveals four $CD11b^{++}F4/80^{++}$ Mφ subsets at resolution (72 hours): (P3) YFP^- resident (embryonic, YFP^-PKH^+ [$M\varphi s^{TR\text{-}inflam}$]) and (P4) YFP^- inflammation-induced Mφs (monocyte-derived ,YFP^-PKH^- [mo-$M\varphi s^{inflam}$]) along with two groups of pro-B cell-derived YFP^+ Mφs generated during homeostasis namely (P5) resident pB-Mφs (YFP^+PKH^+ [pB-$M\varphi s^{TR\text{-}inflam}$]) and (P6) inflammation-induced pB-Mφs (YFP^+PKH^- [pB-$M\varphi s^{inflam}$]). The software tool Biolayout *Express*^{3D} was used for the visualization and analysis of Illumina *Mus musculus* 6v2 microarray data, which were variance stabilized (VST) and robust spline normalized (RSN) using the lumi R/BioConductor package. Correlation networks, sample comparison and identification of co-expression modules was performed in Biolayout *Express*^{3D} for 30 data sets (n=3 per group). **b,** Sample similarity analysis diagram showing cell type-specific clustering of datasets. Analysis was performed using Person correlation threshold of $r \geq 0.97$ and MCL clustering algorithm with inflation value of 3.0. Individual clusters of nodes (samples) were arbitrarily assigned a colour. **c**, Network graph generated using Person correlation threshold of $r \geq 0.95$ and MCL clustering algorithm with inflation value of 1.7 is showing clusters of genes correlating in their expression profiles and includes clusters of genes with similar function and/or genes with cell-specific expression pattern. Table S1 provides the content of each of these clusters.

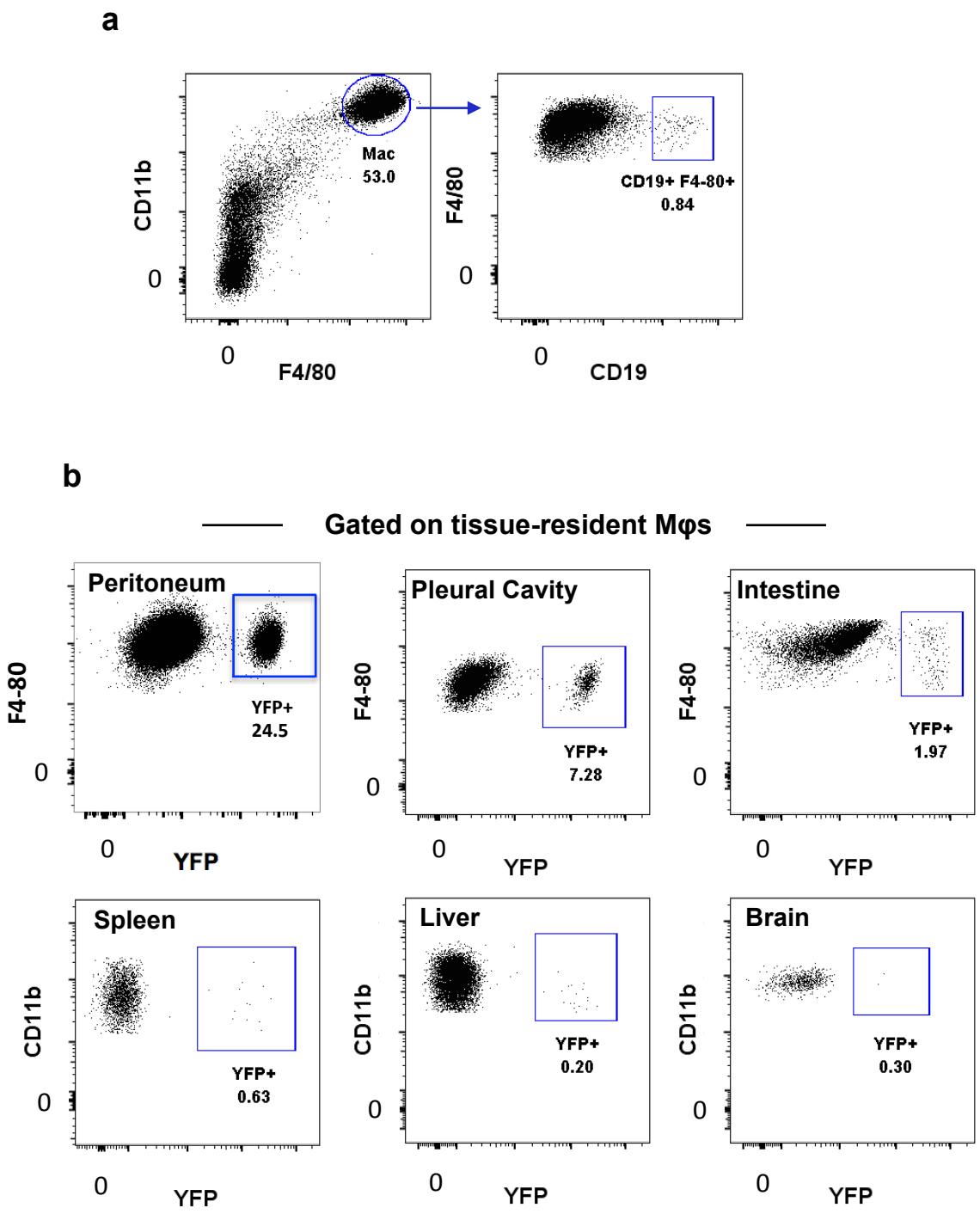
a
CD11b
0
0
F4/80
Mac
53.0
F4/80
0
0
CD19
CD19+ F4-80+
0.84
b
Gated on tissue-resident Mφs
Peritoneum
F4-80
0
0
YFP
YFP+
24.5
Pleural Cavity
F4-80
0
0
YFP
YFP+
7.28
Intestine
F4-80
0
0
YFP
YFP+
1.97
Spleen
CD11b
0
0
YFP
YFP+
0.63
Liver
CD11b
0
0
YFP
YFP+
0.20
Brain
CD11b
0
0
YFP
YFP+
0.30

a

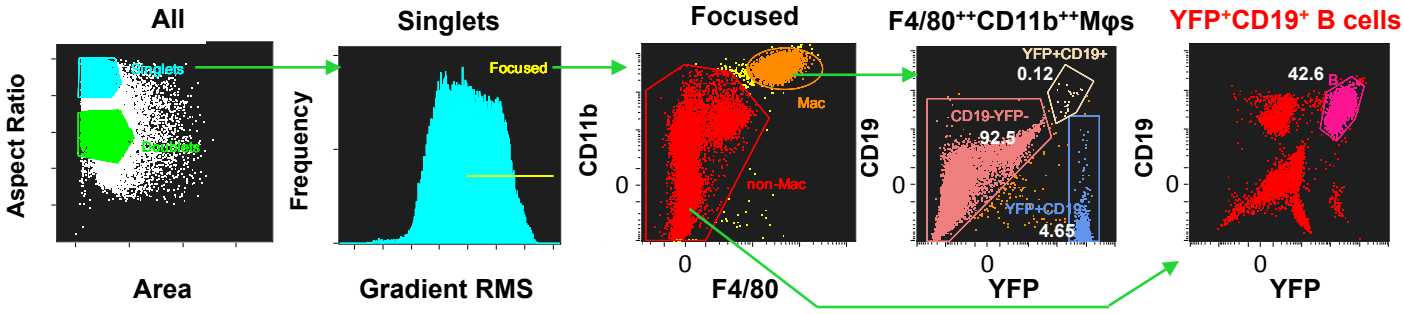

b

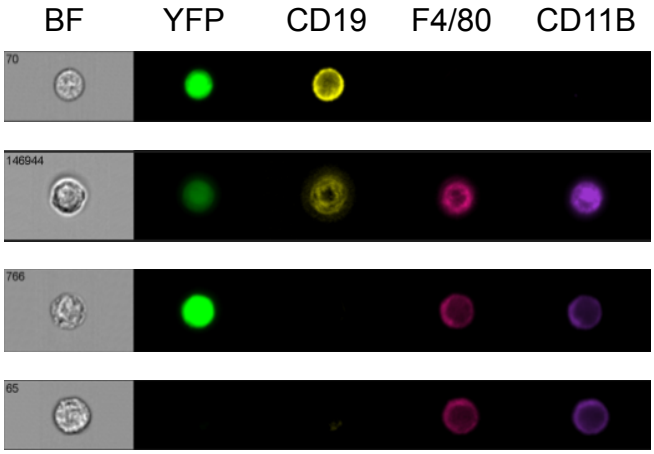

Sample number	% of single YFP+ CD19+ Mφs
1	9.68
2	14.46
3	26.09
Average	16.74

c

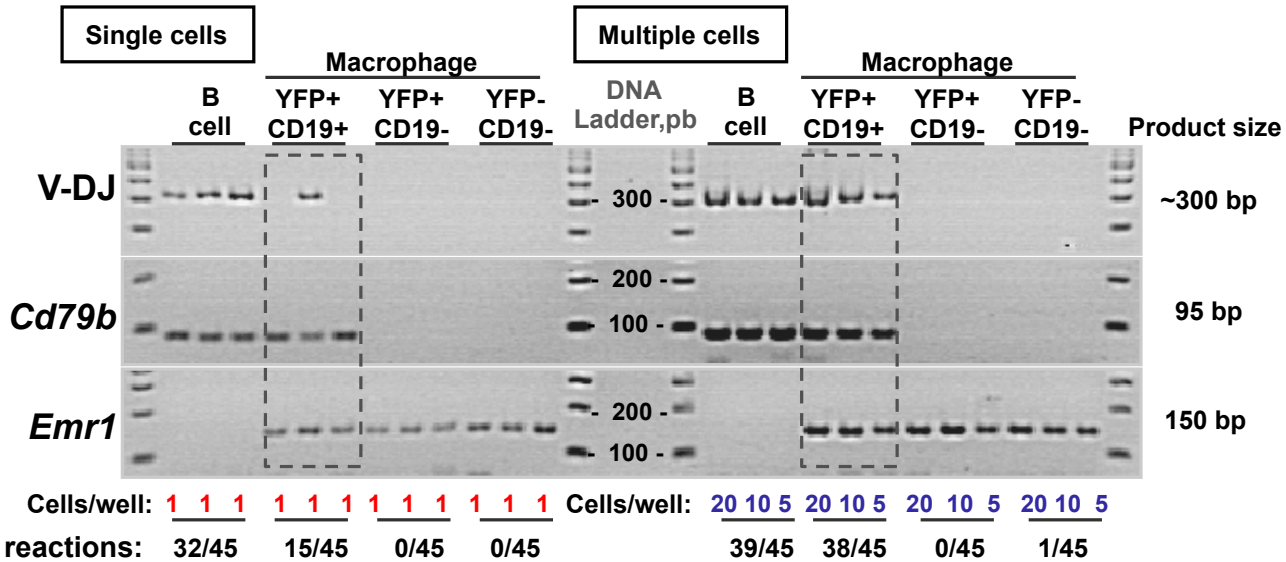

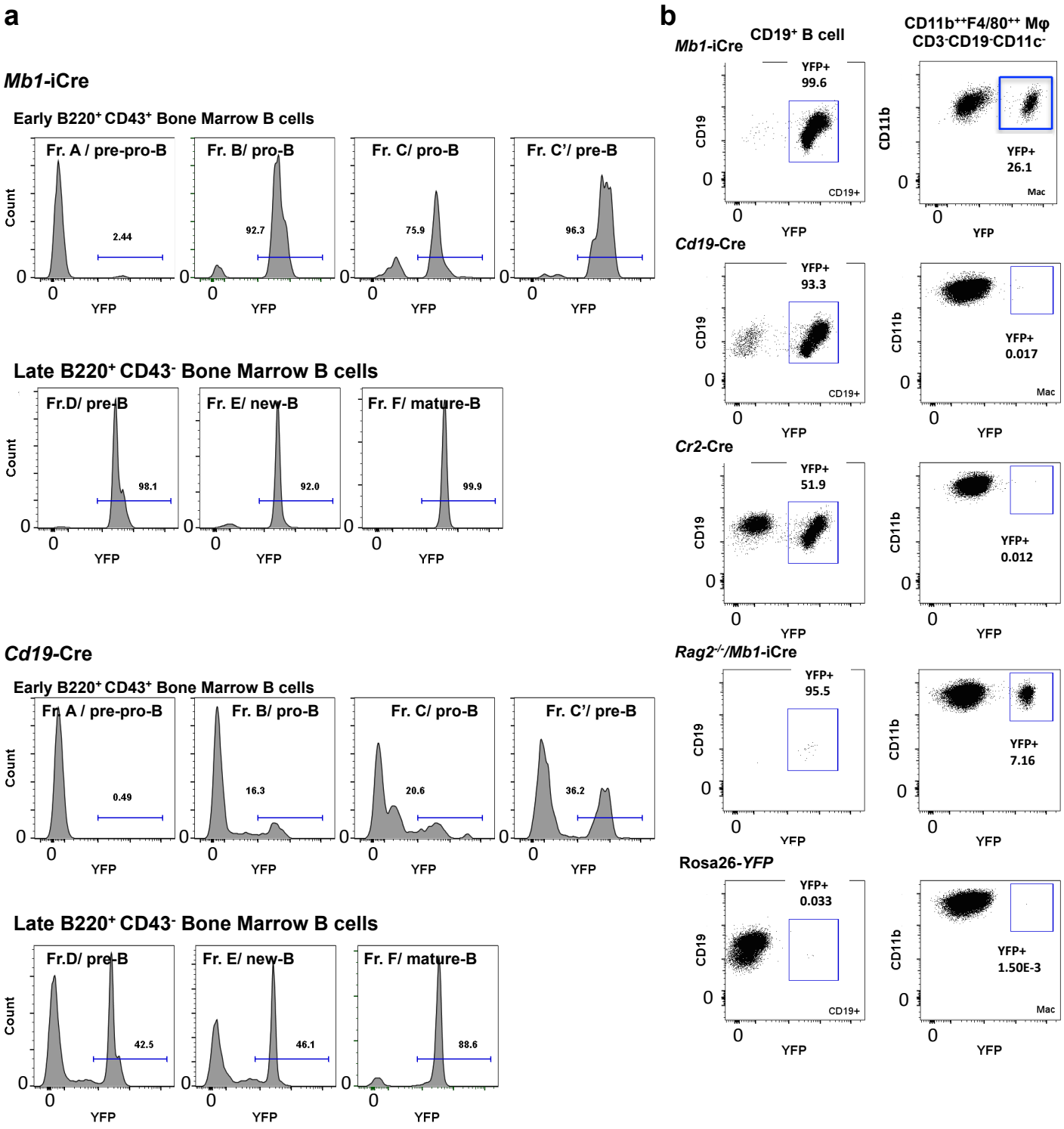
a
Mb1-iCre
Early B220+ CD43+ Bone Marrow B cells
Fr. A / pre-pro-B
Fr. B/ pro-B
Fr. C/ pro-B
Fr. C'/ pre-B
Count
2.44
92.7
75.9
96.3
YFP
Late B220+ CD43- Bone Marrow B cells
Fr.D/ pre-B
Fr. E/ new-B
Fr. F/ mature-B
98.1
92.0
99.9
Cd19-Cre
Early B220+ CD43+ Bone Marrow B cells
0.49
16.3
20.6
36.2
Late B220+ CD43- Bone Marrow B cells
42.5
46.1
88.6
b
Mb1-iCre
CD19+ B cell
CD11b++F4/80++ Mφ
CD3-CD19-CD11c-
CD19
CD11b
YFP+
99.6
26.1
CD19+
Mac
Cd19-Cre
93.3
0.017
Cr2-Cre
51.9
0.012
Rag2-/-/Mb1-iCre
95.5
7.16
Rosa26-YFP
0.033
1.50E-3

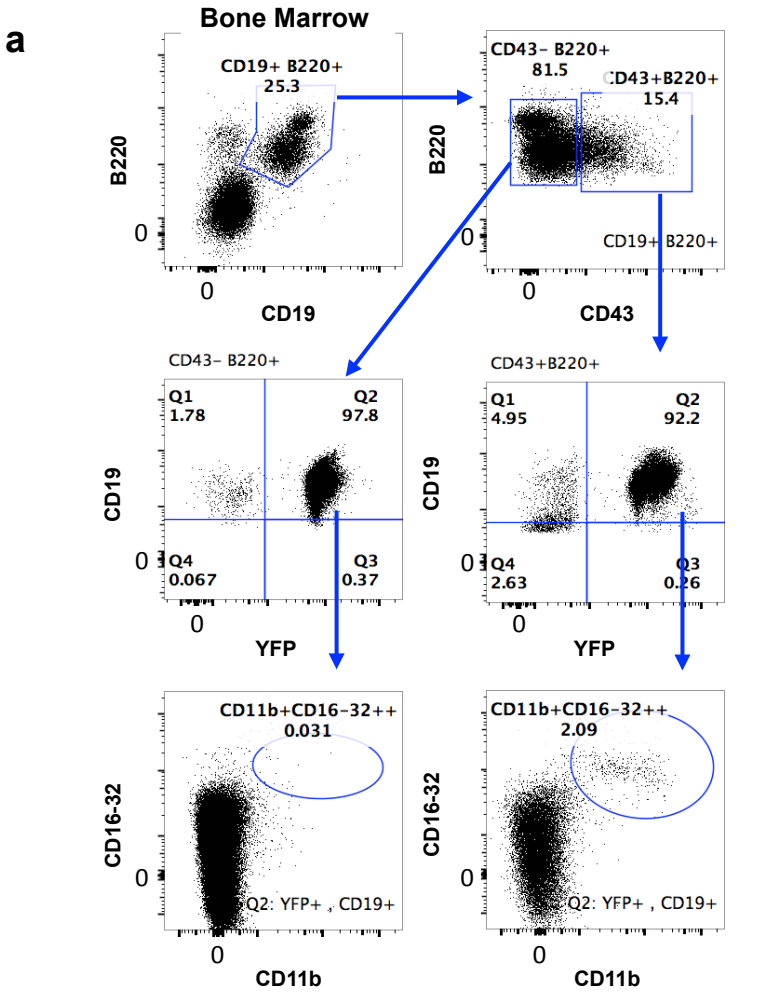
a
Bone Marrow
CD19+ B220+
25.3
B220
CD19
CD43- B220+
81.5
CD43+B220+
15.4
CD43
CD19+ B220+
CD43- B220+
Q1
1.78
Q2
97.8
Q4
0.067
Q3
0.37
YFP
CD43+B220+
Q1
4.95
Q2
92.2
Q4
2.63
Q3
0.26
YFP
CD11b+CD16-32++
0.031
CD16-32
Q2: YFP+ , CD19+
CD11b
CD11b+CD16-32++
2.09
CD16-32
Q2: YFP+ , CD19+
CD11b

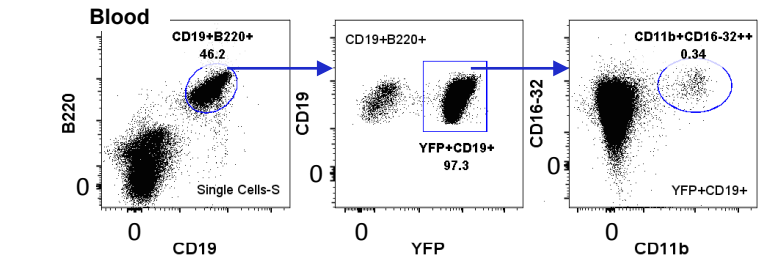
b
Blood
CD19+B220+
46.2
B220
Single Cells-S
CD19
CD19+B220+
YFP+CD19+
97.3
YFP
CD16-32
CD11b+CD16-32++
0.34
YFP+CD19+
CD11b

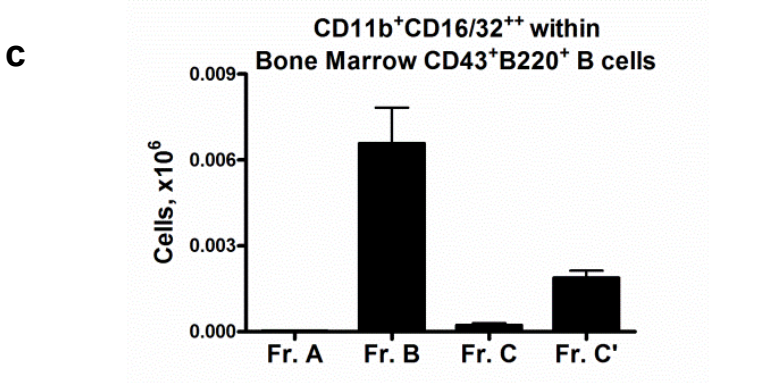
c
CD11b+CD16/32++ within
Bone Marrow CD43+B220+ B cells
Cells, x10^6
0.009
0.006
0.003
0.000
Fr. A
Fr. B
Fr. C
Fr. C'

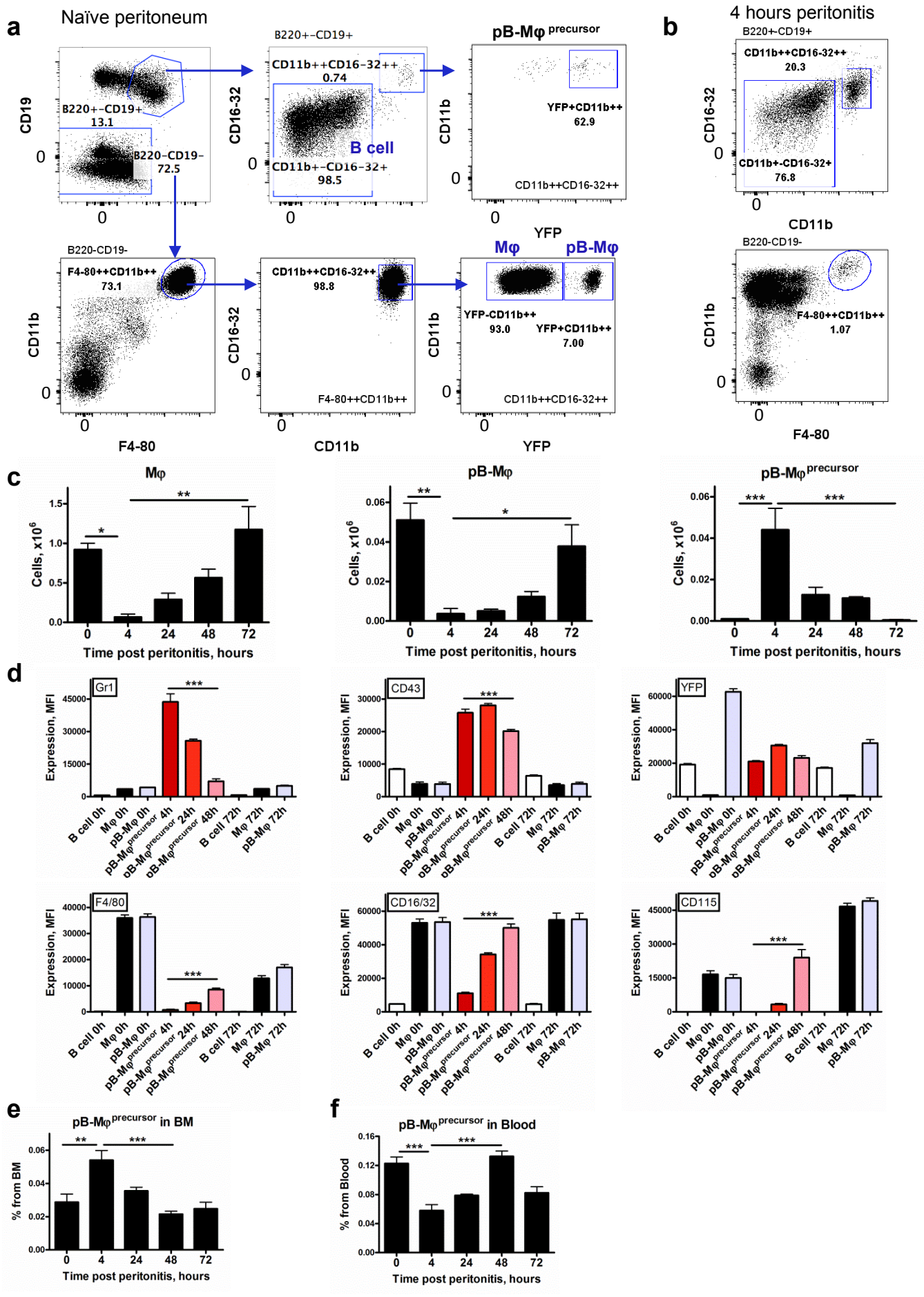
a
Naïve peritoneum
B220+-CD19+
13.1
B220-CD19-
72.5
CD19
CD16-32
CD11b
B220+-CD19+
CD11b++CD16-32++
0.74
B cell
CD11b+-CD16-32+
98.5
pB-Mφ precursor
YFP+CD11b++
62.9
CD11b++CD16-32++
B220-CD19-
F4-80++CD11b++
73.1
CD11b++CD16-32++
98.8
F4-80++CD11b++
YFP
Mφ
pB-Mφ
YFP-CD11b++
93.0
YFP+CD11b++
7.00
CD11b++CD16-32++
F4-80
CD11b
YFP
b
4 hours peritonitis
B220+-CD19+
CD11b++CD16-32++
20.3
CD11b+-CD16-32+
76.8
CD16-32
CD11b
B220-CD19-
F4-80++CD11b++
1.07
CD11b
F4-80
c
Mφ
pB-Mφ
pB-Mφ precursor
Cells, x10^6
Time post peritonitis, hours
0
4
24
48
72
d
Gr1
CD43
YFP
F4/80
CD16/32
CD115
Expression, MFI
B cell 0h
Mφ 0h
pB-Mφ 0h
pB-Mφ precursor 4h
pB-Mφ precursor 24h
pB-Mφ precursor 48h
B cell 72h
Mφ 72h
pB-Mφ 72h
e
pB-Mφ precursor in BM
% from BM
Time post peritonitis, hours
f
pB-Mφ precursor in Blood
% from Blood
Time post peritonitis, hours

a

CMPs		proB cells		pB-Mϕ precursors	
Myeloid	lymphoid	Myeloid	lymphoid	Myeloid	lymphoid
2130±103 out of 2500 events (n=5 wells seeded with single cells)	ND	ND	2178±445 out of 2500 events (n=5 wells seeded with single cells)	1875±397 out of 2500 events (n=5 wells seeded with single cells)	74±21 out of 500 events (n=5 wells seeded with single cells)

b

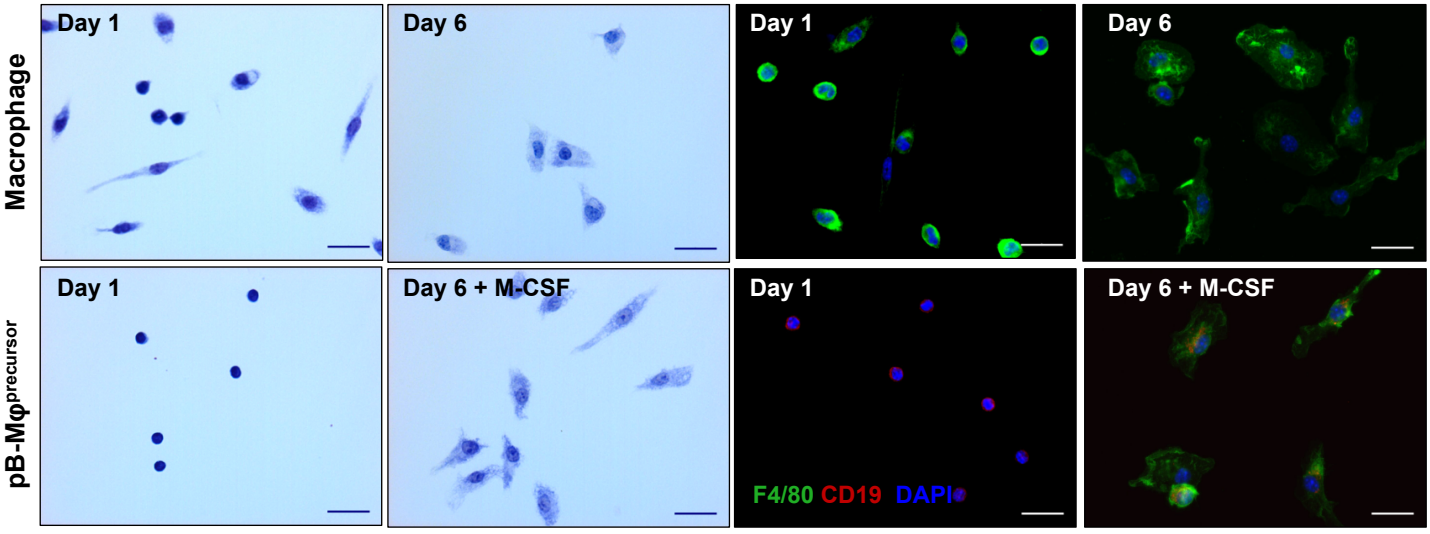

c

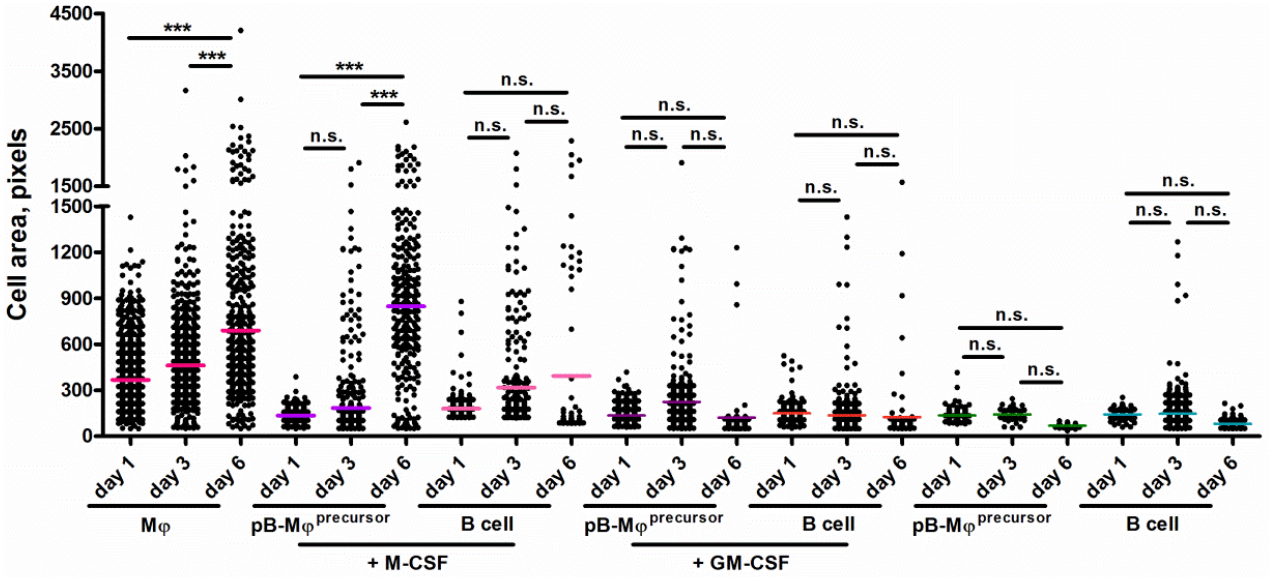

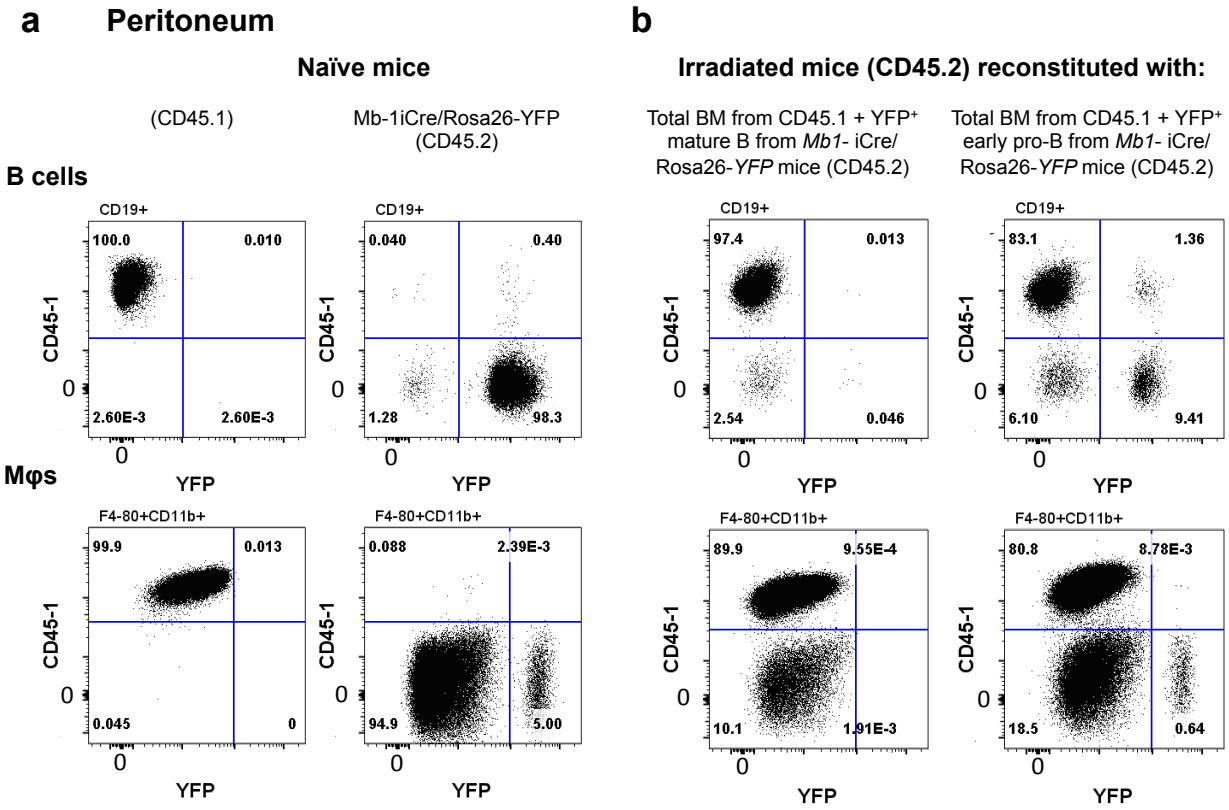
a
Peritoneum
Naïve mice
(CD45.1)
Mb-1iCre/Rosa26-YFP
(CD45.2)
B cells
Mφs
CD19+
F4-80+CD11b+
CD45-1
YFP
100.0
0.010
2.60E-3
2.60E-3
0.040
0.40
1.28
98.3
99.9
0.013
0.045
0
0.088
2.39E-3
94.9
5.00
b
Irradiated mice (CD45.2) reconstituted with:
Total BM from CD45.1 + YFP+ mature B from Mb1- iCre/ Rosa26-YFP mice (CD45.2)
Total BM from CD45.1 + YFP+ early pro-B from Mb1- iCre/ Rosa26-YFP mice (CD45.2)
97.4
0.013
2.54
0.046
83.1
1.36
6.10
9.41
89.9
9.55E-4
10.1
1.91E-3
80.8
8.78E-3
18.5
0.64

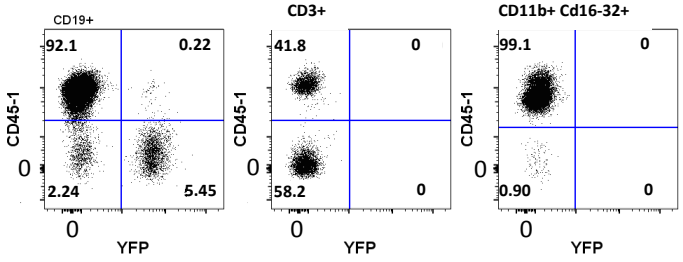
c
Spleen
Irradiated mice (CD45.2) reconstituted with:
Total BM from CD45.1 + YFP+ early pro-B from Mb1- iCre/Rosa26-YFP mice (CD45.2)
CD19+
CD3+
CD11b+ Cd16-32+
CD45-1
YFP
92.1
0.22
2.24
5.45
41.8
0
58.2
0
99.1
0
0.90
0

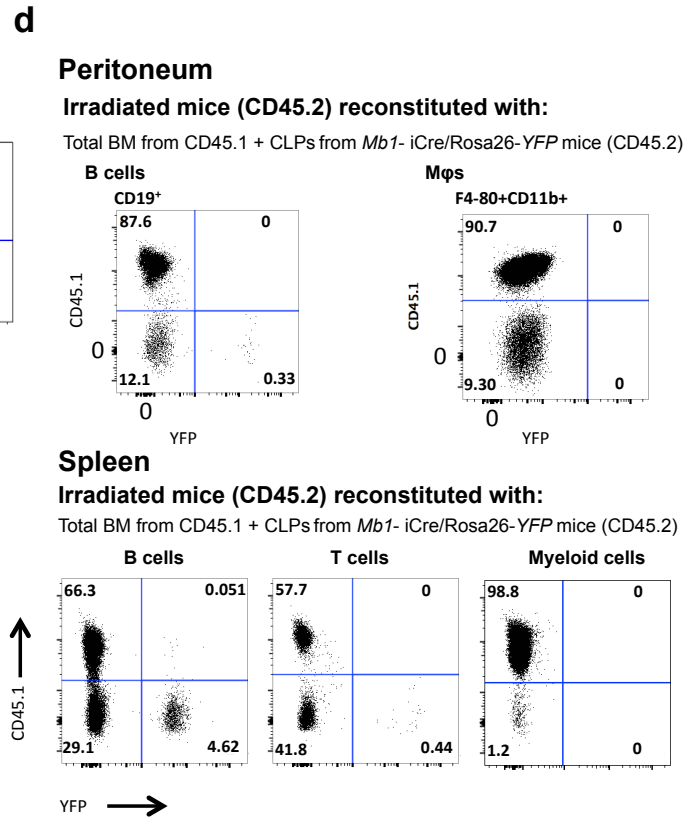
d
Peritoneum
Irradiated mice (CD45.2) reconstituted with:
Total BM from CD45.1 + CLPs from Mb1- iCre/Rosa26-YFP mice (CD45.2)
B cells
CD19+
Mφs
F4-80+CD11b+
CD45.1
YFP
87.6
0
12.1
0.33
90.7
0
9.30
0
Spleen
Irradiated mice (CD45.2) reconstituted with:
Total BM from CD45.1 + CLPs from Mb1- iCre/Rosa26-YFP mice (CD45.2)
B cells
T cells
Myeloid cells
66.3
0.051
29.1
4.62
57.7
0
41.8
0.44
98.8
0
1.2
0

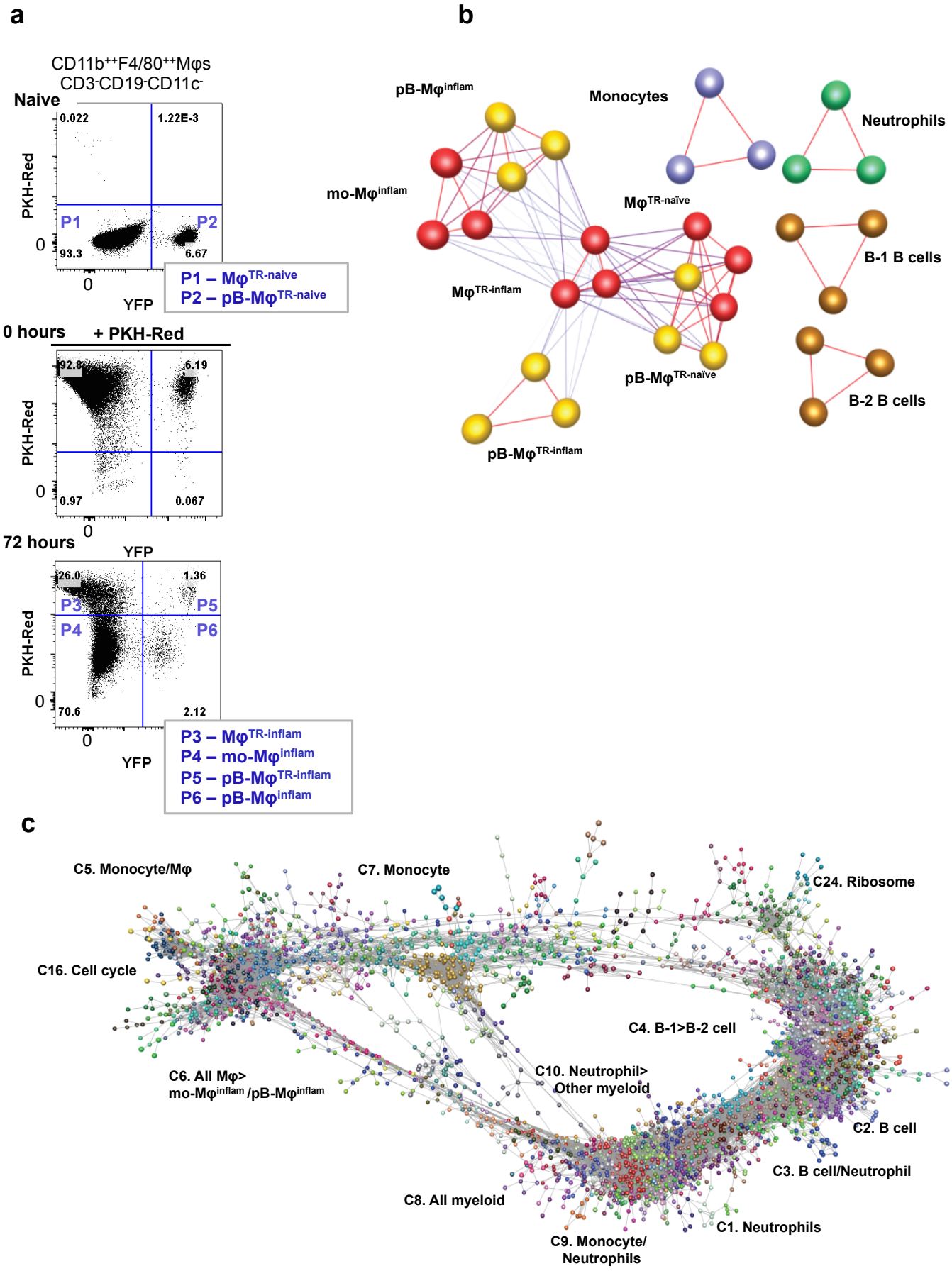
a
CD11b++F4/80++Mφs
CD3-CD19-CD11c-
Naive
0.022
1.22E-3
P1
P2
93.3
6.67
PKH-Red
YFP
P1 – MφTR-naive
P2 – pB-MφTR-naive
0 hours
+ PKH-Red
92.8
6.19
0.97
0.067
72 hours
26.0
1.36
P3
P5
P4
P6
70.6
2.12
P3 – MφTR-inflam
P4 – mo-Mφinflam
P5 – pB-MφTR-inflam
P6 – pB-Mφinflam
b
pB-Mφinflam
Monocytes
Neutrophils
mo-Mφinflam
MφTR-naïve
B-1 B cells
MφTR-inflam
pB-MφTR-naïve
B-2 B cells
pB-MφTR-inflam
c
C5. Monocyte/Mφ
C7. Monocyte
C24. Ribosome
C16. Cell cycle
C4. B-1>B-2 cell
C6. All Mφ>
mo-Mφinflam /pB-Mφinflam
C10. Neutrophil>
Other myeloid
C2. B cell
C3. B cell/Neutrophil
C8. All myeloid
C1. Neutrophils
C9. Monocyte/
Neutrophils

Supplementary Figure 1.1

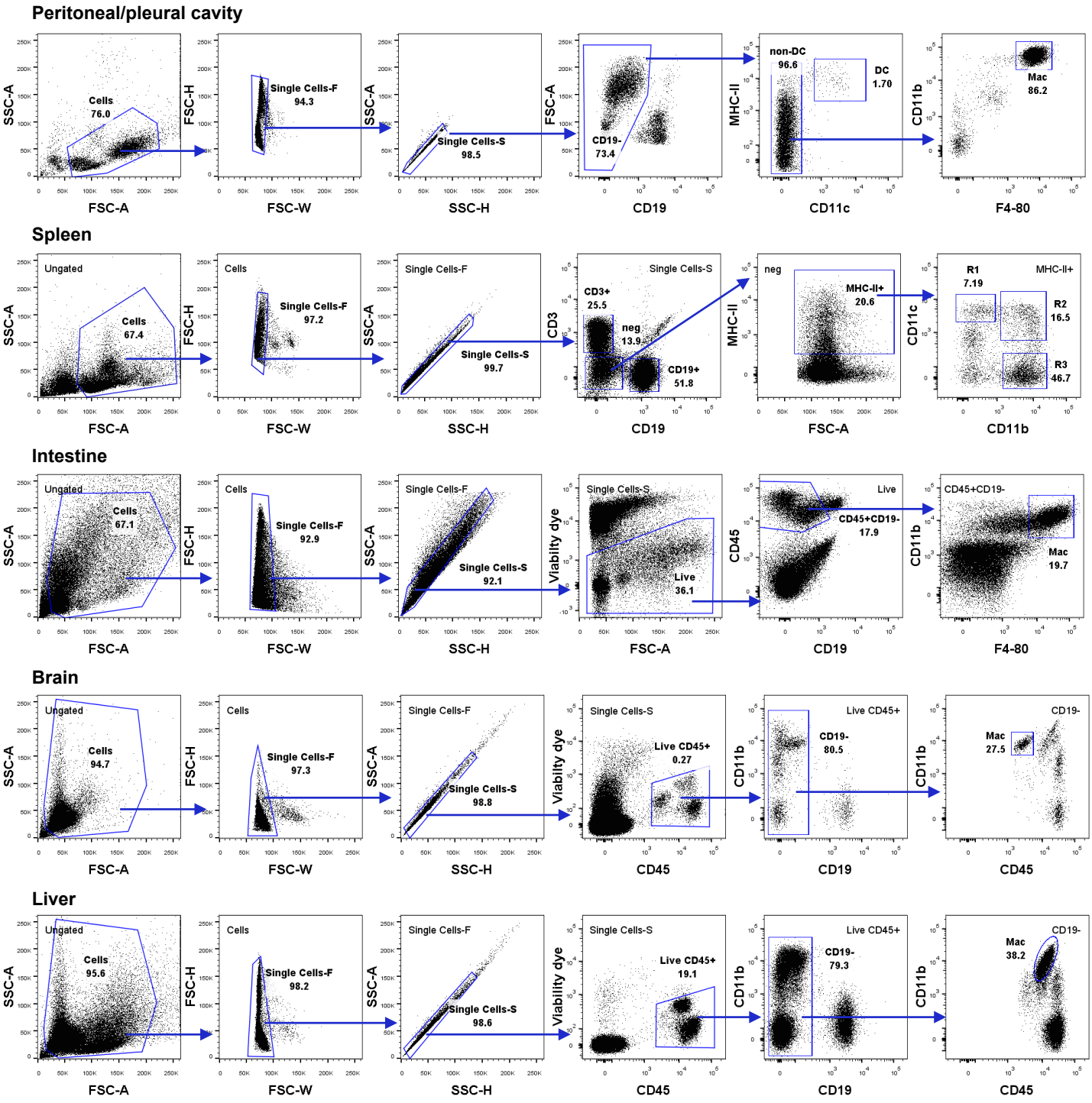

Supplementary Figure 1.1. Gating strategies for flow cytometric identifications of tissue-resident Mφs. a, Tissue-resident Mφs were discriminated from cell debris by size (FSC) and granularity (SSC), followed by cell doublets exclusion using Height (FSC-H/SCC-H), Width (FSC-W) and Area (SCC-A) parameters, and then identified within live cell gate as $CD11b^{++}$ (brain and liver) or as $CD11b^{++}F4/80^{++}$(intestine) cells within $CD45^{+}CD19^{-}$ population. Splenic Mφs were identified as $CD3^{-}CD19^{-}MHC\text{-}II^{+}$ cells, which were $CD11b^{+}CD11c^{-}$(R3) and $F4/80^{+}$(not shown), while peritoneal and pleural cavity Mφs were $CD19^{-}CD11c^{-}CD11b^{++}F4/80^{++}$.

Supplementary Figure 1.2

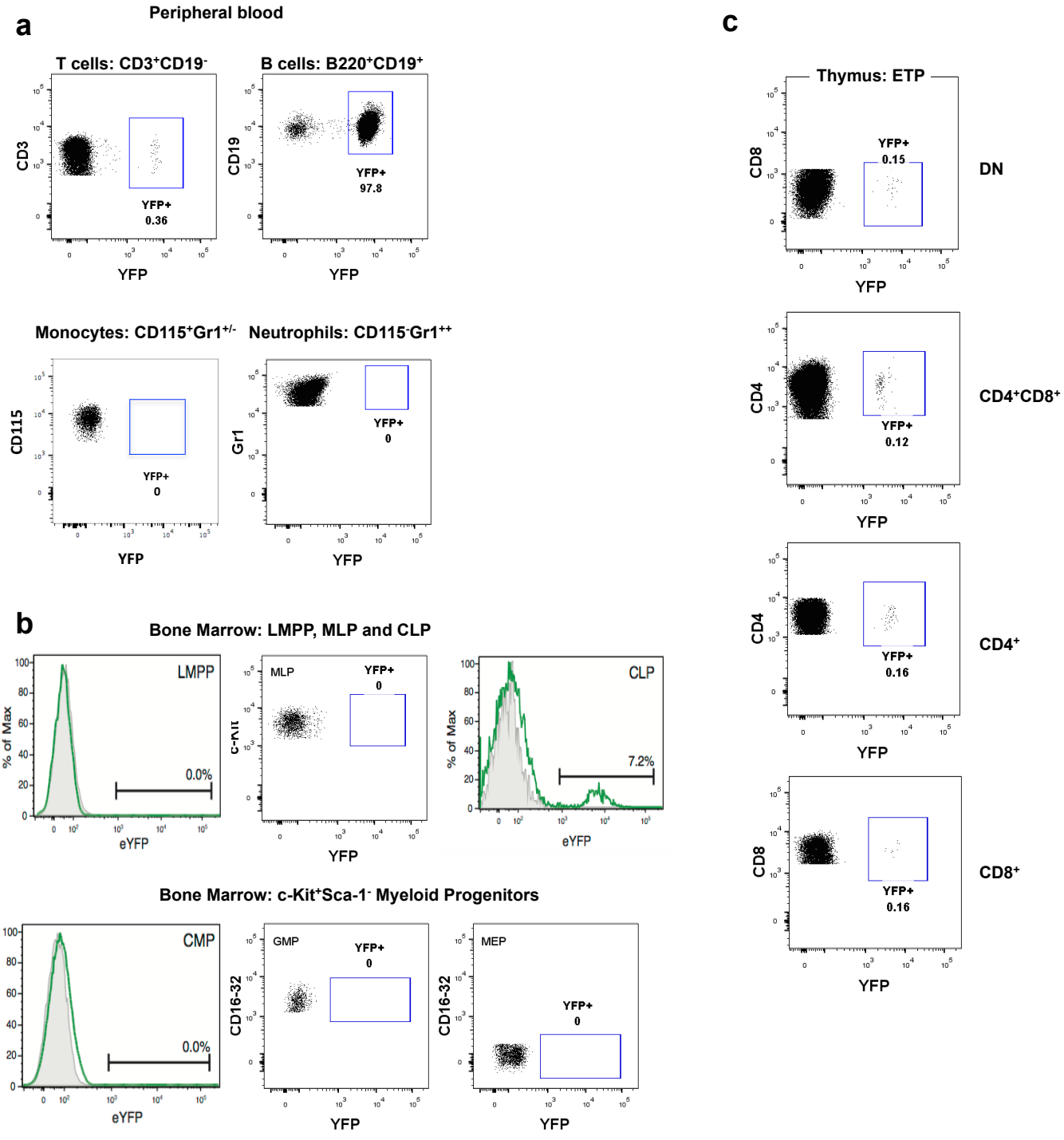

Supplementary Figure 1.2 Analysis of *Mb1*-iCre/Rosa26-*YFP* mice for YFP expression within cells of various organs including (**a**) peripheral blood B and T cells as well as monocytes and neutrophils. Analysis of (**b**) bone marrow hematopoietic precursors revealed some YFP expression in uncommitted common lymphoid progenitors (CLP) only while **(c)** shows YFP expression in thymus.

Supplementary Figure 1.3

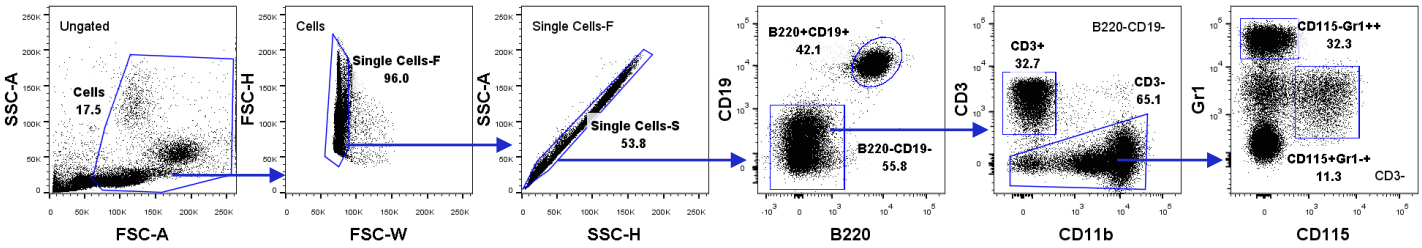

Supplementary Figure 1.3. Gating strategies for flow cytometric identification of peripheral blood cell populations. a, Blood cells were discriminated from cell debris by size (FSC) and granularity (SSC), followed by cell doublets exclusion using Height (FSC-H/SCC-H), Width (FSC-W) and Area(SCC-A) parameters. B cells were identified within $B220^{+}CD19^{+}$ gate, T cells as $CD3^{+}$ within $B220^{-}CD19^{-}$ gate, while neutrophils were $CD115^{-}Gr1^{++}$ and monocytes were $CD115^{+}Gr1^{+/-}$ cells within $B220^{-}CD19^{-}CD3^{-}$ gate.

Supplementary Figure 1.4

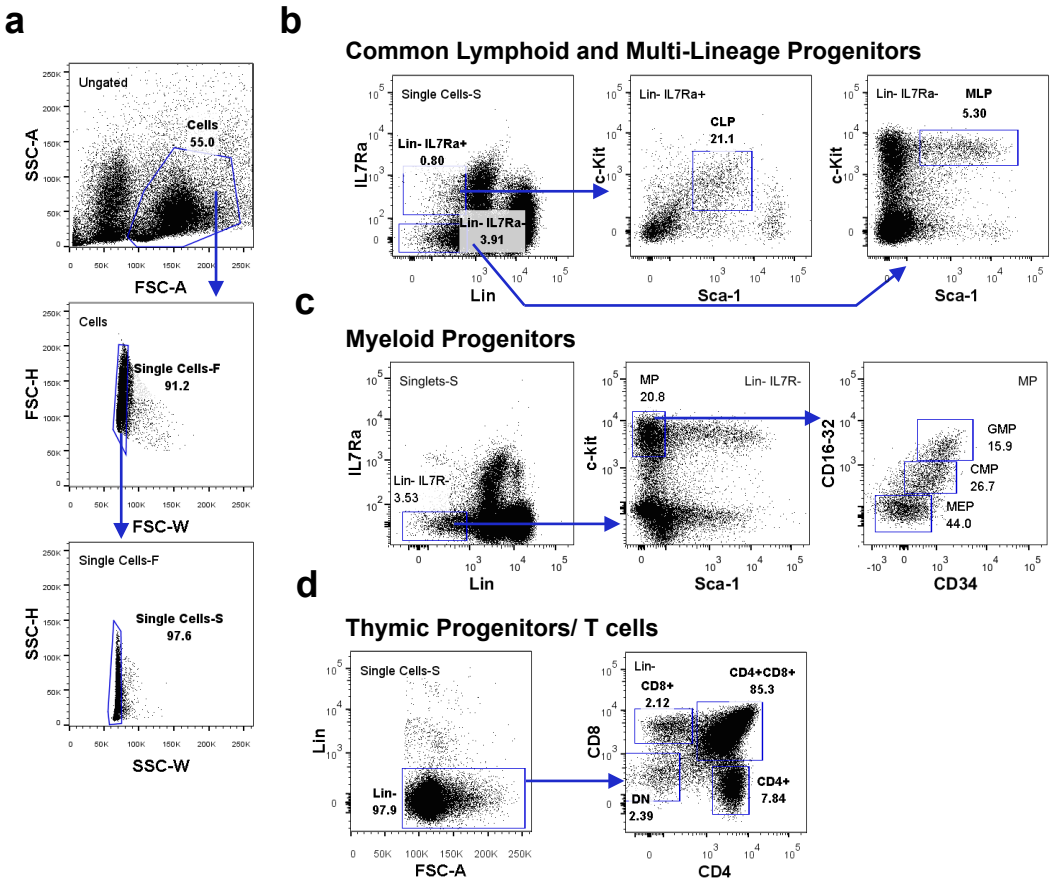

Supplementary Figure 1.4. Gating strategies for flow cytometric identification of hematopoietic progenitors in bone marrow and T cell progenitors in thymus. a, Bone marrow/thymus cells were discriminated from cell debris by size (FSC) and granularity (SSC), followed by cell doublets exclusion using Height (FSC-H/SCC-H), Width (FSC-W/SCC-W) parameters. **b,** Sca-1^{++}c-Kit^{++} multi-lineage progenitors (MLP) and Sca-1^{+}c-Kit^{+} common lymphoid progenitors (CLP) were identified within Lin^{-}IL7Rα^{-} and Lin^{-}IL7Rα^{+} bone marrow fractions respectively. **c,** Sca-1^{-}c-Kit^{++} total myeloid progenitors (MP) were identified within Lin^{-} IL7Rα^{-} bone marrow fraction and were comprised of three populations: CD34$^{+/-}$CD16/32^{+} common myeloid progenitor (CMP), CD34^{+}CD16/32^{++} granulocyte/macrophage progenitor (GMP) and CD34^{-}CD16/32^{-} megakaryocyte/erythrocyte progenitor. **d,** CD4^{-}CD8^{-} (DN) Early Thymic progenitors (ETP) were identified within Lin^{-} fraction of thymic cells, while immature thymocytes CD4^{+}CD8^{+} and mature T cells were either CD4^{+} or CD8^{+}. Lin markers for MLPs and CLPs included CD3, CD4, CD8, B220, CD11b, Gr1, TER119; for MPs - CD3, CD4, CD8, CD19, B220, IgM, CD11b, Gr1, TER119; for ETPs - CD19, B220, CD11b, Gr1, NK1.1, TER119.

Supplementary Figure 2

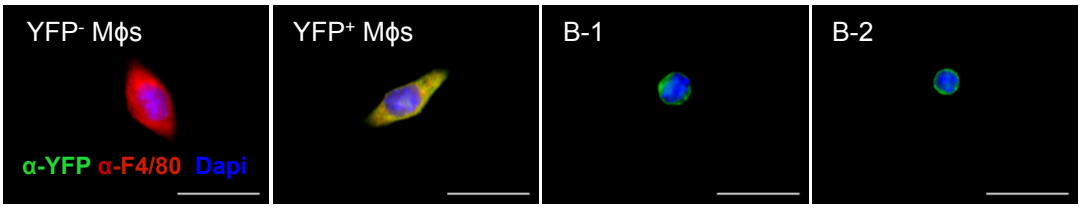

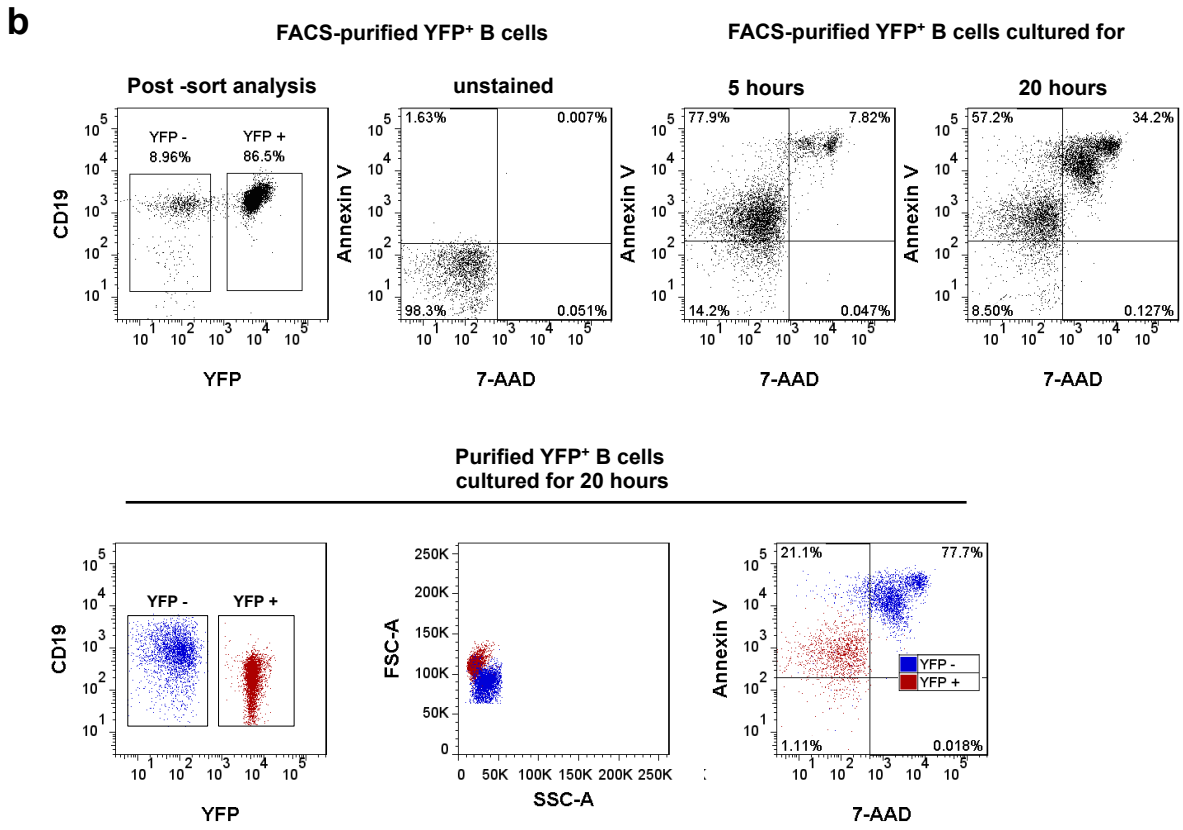

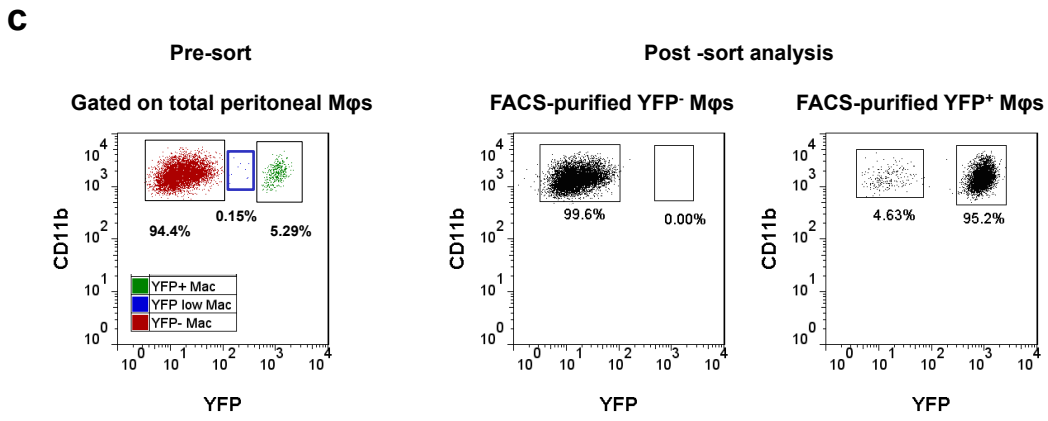

Supplementary Figure 2

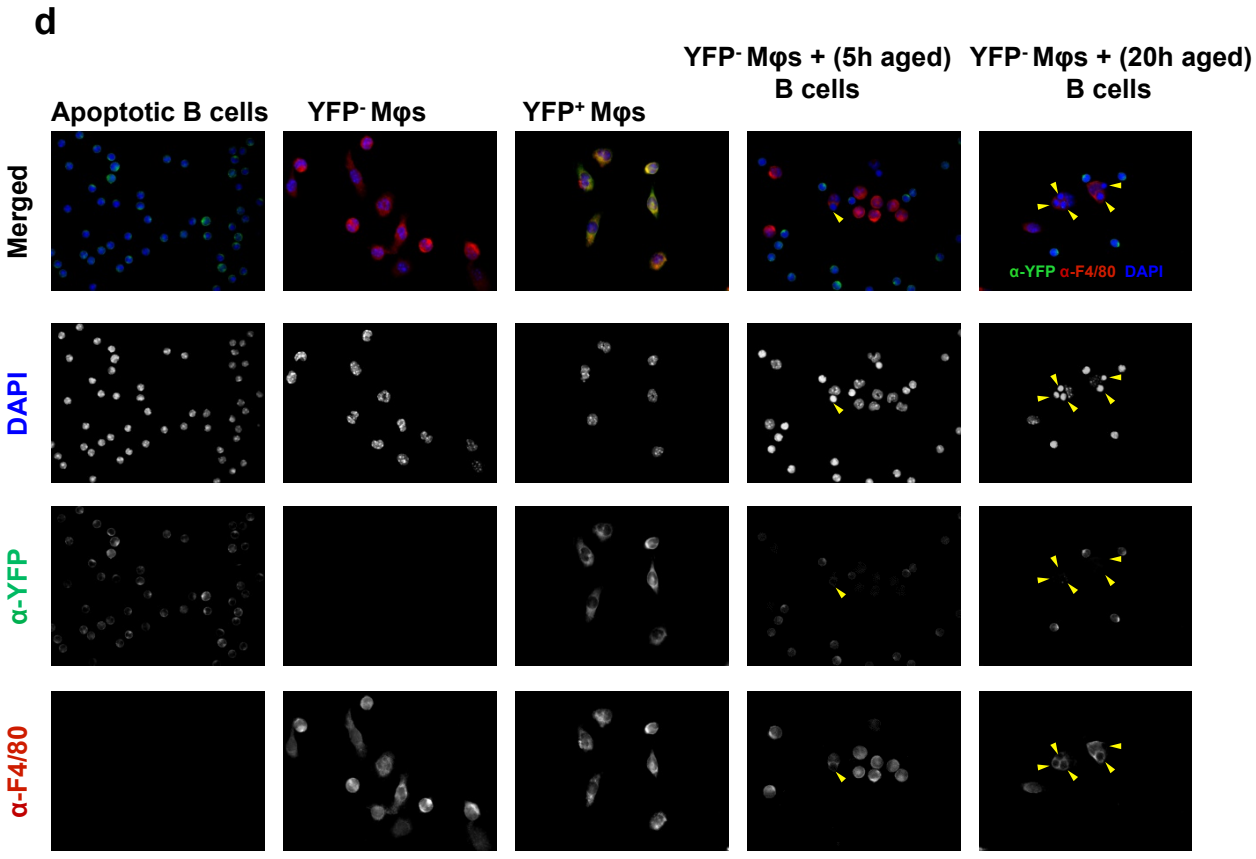

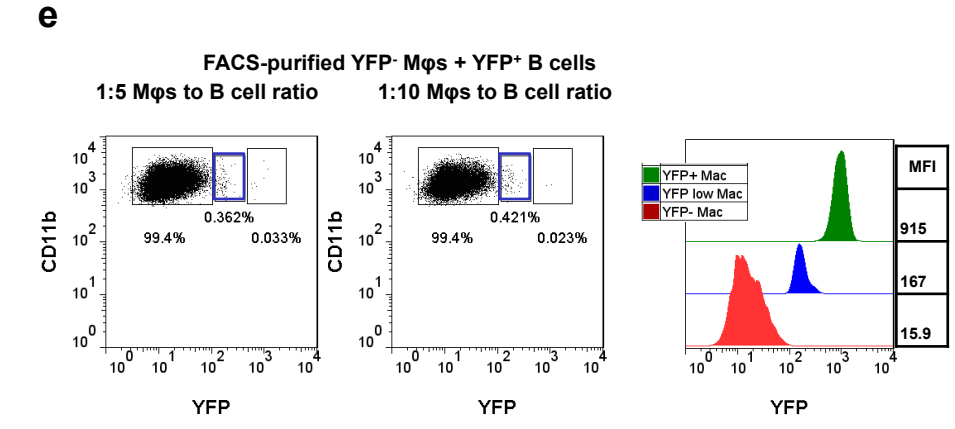

Supplementary Figure 2. Phagocytosis of YFP$^+$ B cells by Mφs does not result in generation of YFP$^+$ Mφs. a, Immunofluorescent microscopy on FACS-purified peritoneal cell populations. **b,** Flow cytometric analysis of splenic YFP$^+$ CD19$^+$ B cells following FACS-purification was carried out immediately after purification and at 5 and 20 hours after culturing in RPMI media supplemented with 5 % FBS, 1000 U/ml penicillin, 1000 µg/ml streptomycin and 2 mM L-glutamine. Upon culturing without stimulation splenic B cells spontaneously undergo apoptosis as determined by Annexin V and 7-AAD staining. Importantly, after 20 hours the loss of the YFP signal from FACS-purified YFP$^+$CD19$^+$ splenic B cells correlated with low forward scatter and double labelling for Annexin V and 7-AAD, which are characteristic of advanced apoptosis. **c,** Dot-plots showing CD11b^{++}F4/80^{++} Mφ pre-sort populations in peritoneal washout: YFP$^+$ Mφs (green), YFP$^-$ Mφs (red) and very few events showing as YFP low (blue); post-sort purity assessment of YFP$^-$ and YFP$^+$ Mφs. FACS-purified peritoneal YFP$^-$ Mφs were co-incubated with 5 or 20 hours-aged splenic YFP$^+$CD19$^+$ B cells for 1 hour and phagocytosis was analysed by (**d**) microscopy where nuclei were visualized by DAPI in blue, α-F4/80 staining in red and α-GFP(YFP) staining highlights YFP$^+$ B cells and YFP$^+$ Mφs in green. Yellow arrow heads highlight phagocytised B cells, as determined by dense DAPI labelling of apoptotic B cell nuclei contrasting with larger Mφ nuclei revealing condensed and relaxed chromatin structures. **e,** Flow cytometric analysis following co-culturing of YFP$^-$ Mφs with aged splenic B cells revealed only a minor population of Mφs (in blue gate) with increased YFP signal. Histogram showing YFP signal expressed as mean fluorescence intensity (MFI) confirms that population of YFP$^-$ Mφs that have phagocytised YFP$^+$ B cells doesn't gain YFP signal comparable to YFP signal detected in YFP$^+$ Mφs of *Mb1*-iCre/Rosa26-*YFP* mice.

Supplementary Figure 3.1

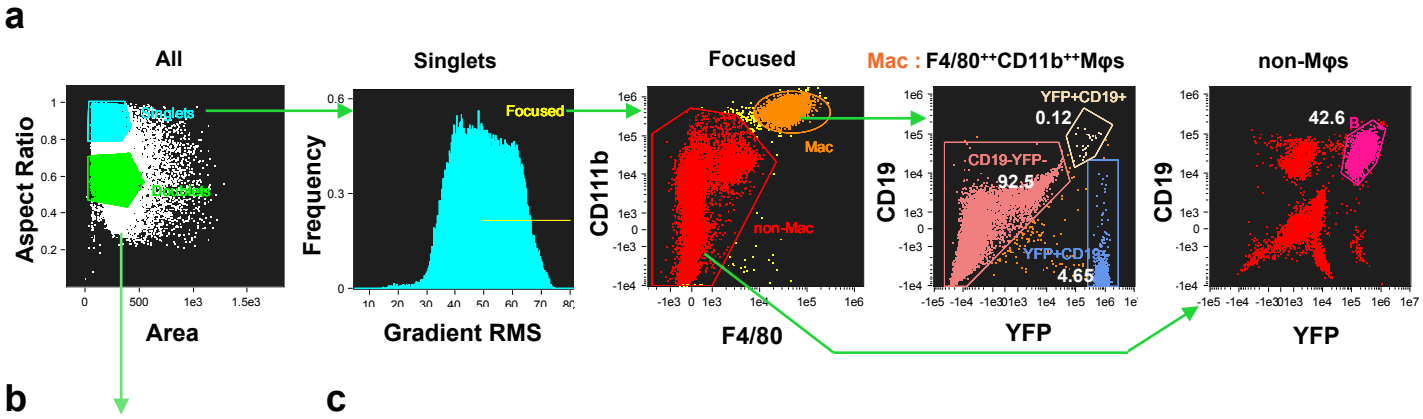

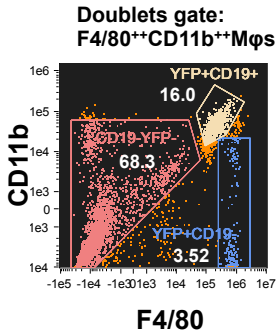

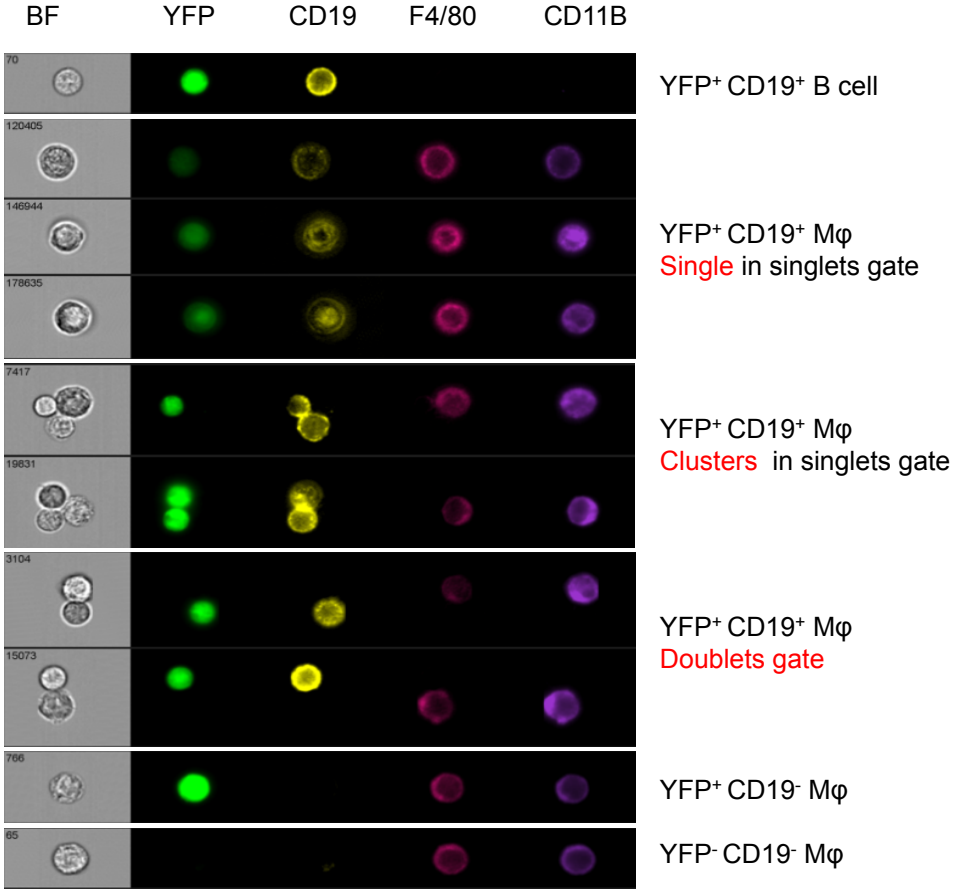

Supplementary Figure 3.1 ImageStream analysis of peritoneal bi-phenotypic YFP^{+}CD19^{+} Mφs in *Mb1*-iCre/Rosa26-*YFP* mice. a, Single cells were discriminated from doublets by Aspect ratio and Area parameters. Mφs were identified as CD11b^{++}F4/80^{++} cells (Mac) within single focused cell gate while B cells are YFP^{+}CD19^{+} population within non-Mφ gate. **b,** Dot plot showing increased frequency of YFP^{+}CD19^{+} population in the CD11b^{++}F4/80^{++} Mφ gate, when gated on focused *doublets*. **c,** Representative images of cell populations gated as above confirming CD19 expression on a sub-population of YFP^{+} Mφs, but showing that Aspect ratio and Area parameters do not allow to exclude all cell clusters and specifically those that have width to heights ratio close to 1, as shown for YFP^{+}CD19^{+} Mφ population clusters in singlets gate.

Supplementary Figure 4.1

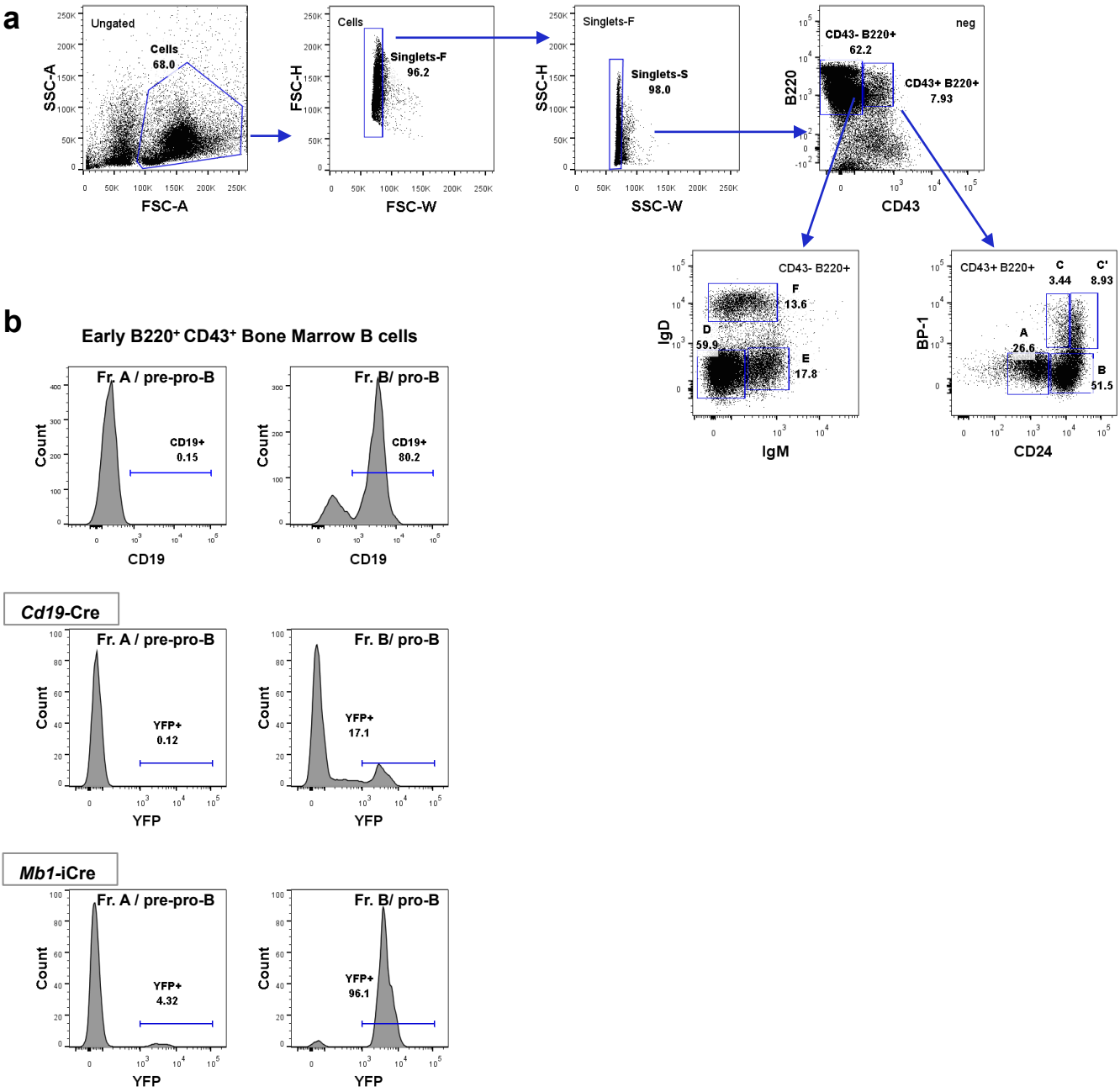

Supplementary Figure 4.1 Gating strategy for flow cytometric identification of B cell development stages in bone marrow. a, Bone marrow cells were discriminated from cell debris by size (FSC) and granularity (SSC), followed by cell doublets exclusion using Heights (FSC-H/SCC-H), Width (FSC-W/SCC-W) parameters. Early B220^{+}CD43^{+} and late B220^{+}CD43^{-} B cell development stages were identified within CD11b^{-}CD3^{-} gate. Early B cells were separated into fractions A, B, C and C' using CD24/HSA and PB-1/Ly-51 antigens: with fraction A being pre-pro-B cells, fraction B and C – pro-B cells and fraction C' – pre-B cells. B220^{+}CD43^{-} B cells comprised of fractions D (pro-B), E (new-B) and F (mature B) discriminated by IgM and IgD expression. **b,** Despite CD19 being expressed on the majority of fraction B/pro-B cells, YFP levels in this early B cell subset of *CD19*-Cre/Rosa26-*YFP* mice (***CD19-Cre***) are very low compared to those detected in *Mb1*-iCre/Rosa26-*YFP* mice (***Mb1*-iCre**).

Supplementary Figure 4.2

a

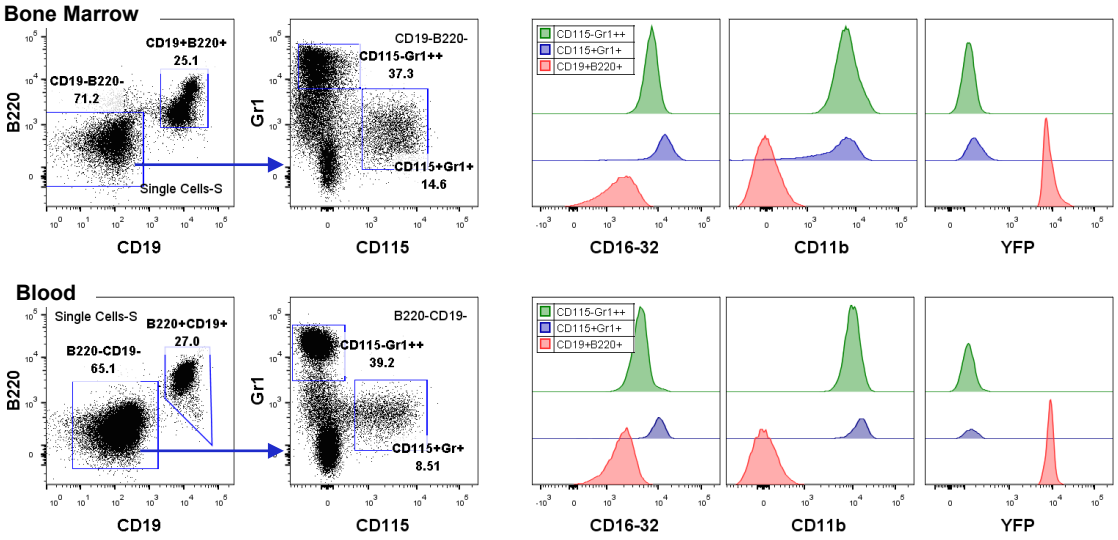

Supplementary Figure 4.2 High CD16/32 and CD11b expression intrinsic to myeloid cells. **a,** Flow cytometry analysis of bone marrow and peripheral blood cell populations revealed high levels of CD16/32 and CD11b on myeloid cells: $Gr1^{++}CD115^{-}$ granulocytes and $Gr1^{+}CD115^{+}$ monocytes in contrast to $B220^{+}CD19^{+}$ B cells.

Supplementary Figure 4.3

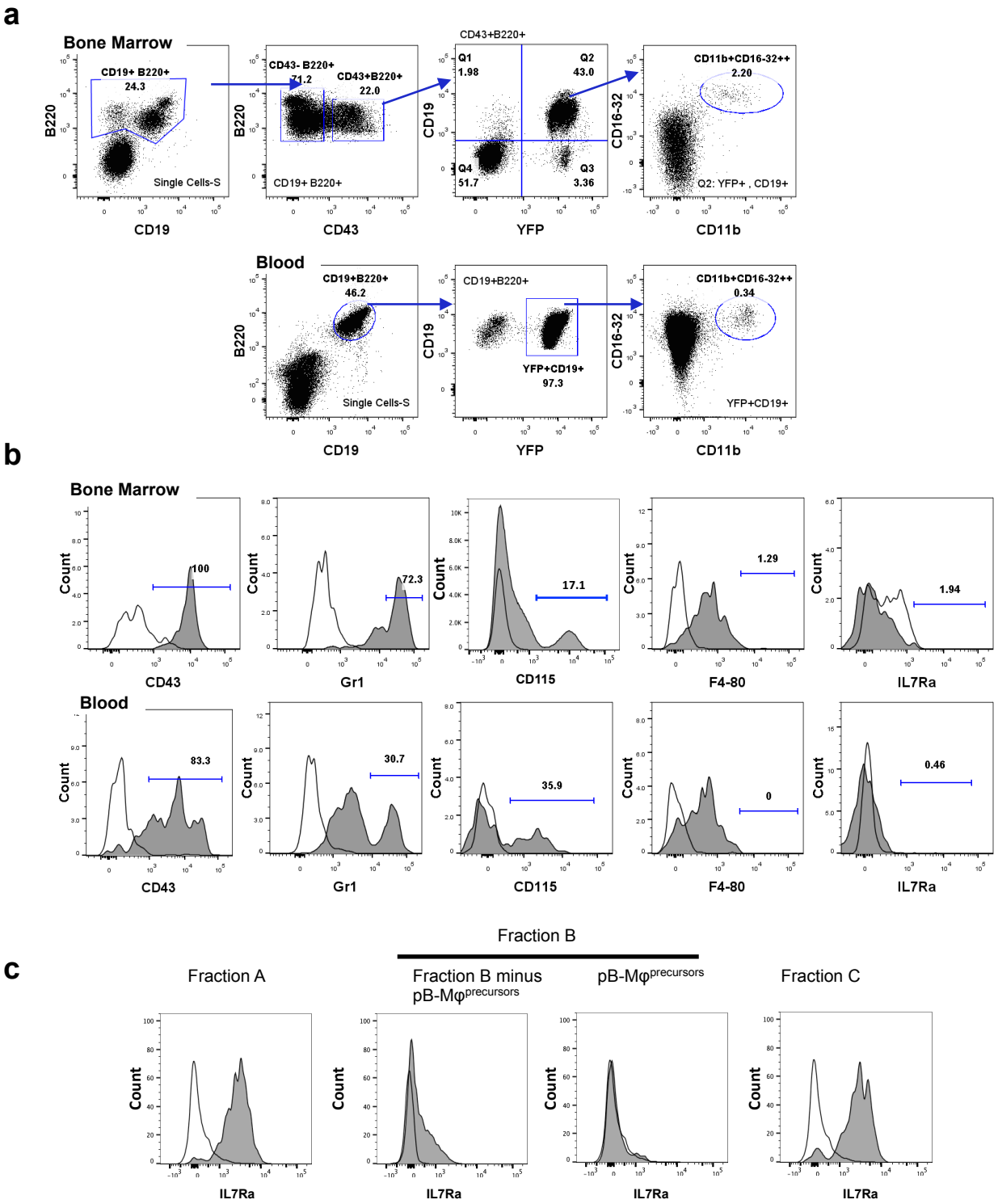

Supplementary Figure 4.3 Cell surface characteristics of bi-phenotypic pB-Mφ^{precursors} in naïve bone marrow and blood. Cells and tissues from *Mb1*-iCre/Rosa26-*YFP* mice were collected and analysed by flow cytometry. **a,** Bi-phenotypic pB-Mφ^{precursors} with B cell and myeloid characteristics namely CD19^{+}B220^{+}CD43^{+}YFP^{+}CD16/32^{++}CD11b^{+} were identified in bone marrow and blood. **b,** Expression pattern of selected cell surface markers on pB-Mφ^{precursors} from naive bone marrow and blood with **c** showing the expression on IL7Ra during the early phases of B cell development.

Supplementary Figure 5.1

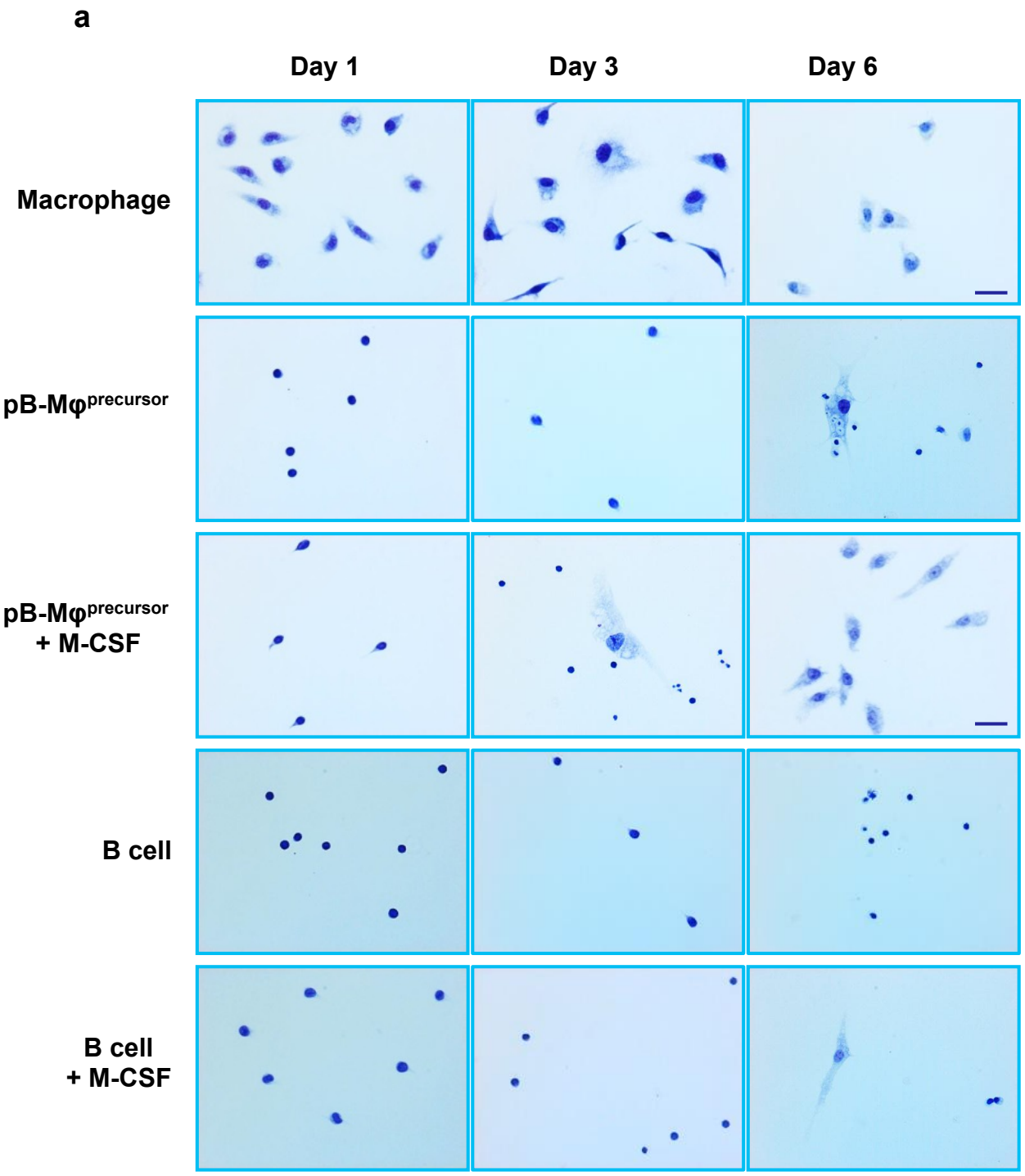

Supplementary Figure 5.2. Morphological changes in pB-Mφ^{precursors} and Mφs during *in vitro* cell culturing. FACS-purified Mφs, peritoneal B cells and peritoneal pB-Mφ^{precursors} from 4 hour peritonitis were cultured on poly-L-lysine-coated coverslips with/without M-CSF for 1, 3, and 6 days. **a,** Rapid-Romanowsky stain revealed typical morphology of B cells for pB-Mφ^{precursors} characterized by high nuclear-cytoplasmic ratio and small cell size, while elongated/ spindle-shaped Mφs had significantly lower nuclear-cytoplasmic ratio and greater cell size at day 1. Upon culturing in presence of 10ng/ml M-CSF majority of pB-Mφ^{precursors} acquired morphology characteristic for Mφs, while B cells and pB-Mφ^{precursors} without M-CSF remained small and round cells. Scale bars, 20 µm.

Supplementary Figure 6.1

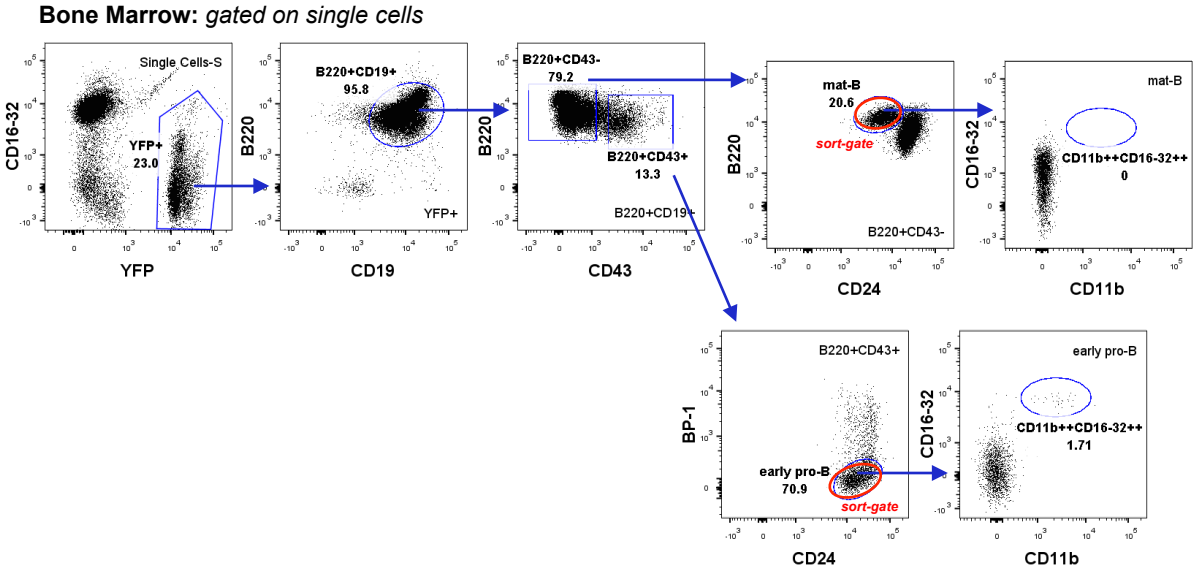

Supplementary Figure 6.1. Gating strategy for isolation of early pro-B and mature B cells from bone marrow of *Mb1*-iCre/Rosa26R-*YFP* mice. Mature B cells ($YFP^{+}B220^{high}CD19^{+}CD43^{-}CD24^{low}$) and early pro-B /Fr. B cells ($YFP^{+}B220^{+}CD19^{+}CD43^{+}CD24^{+}BP\text{-}1^{-}$) from bone marrow of *Mb1*-iCre/Rosa26-*YFP* mice were FACS-purified as shown and injected into lethally irradiated mice to trace the reconstitution of tissue Mφ populations by bi-phenotypic $YFP^{+}CD16/32^{++}CD11b^{++}$ pB-$M\varphi^{precursors}$ within early pro-B cell fraction.

Supplementary Figure 6.2

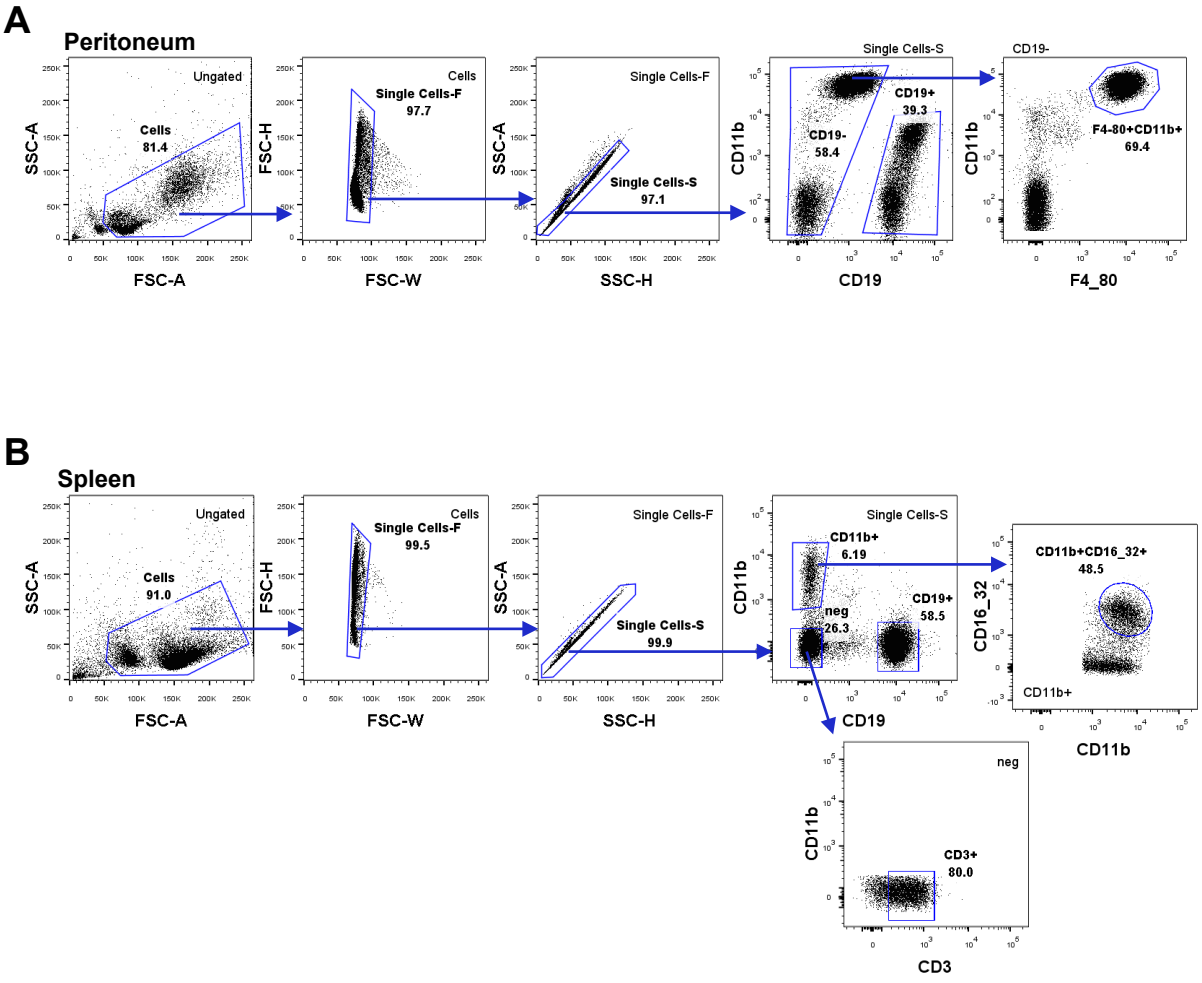

Supplementary Figure 6.2

Supplementary Figure 6.2. YFP^{+}CD16/32^{++}CD11b pB-Mφ^{precursors} within early pro-B cell bone marrow fraction reconstitute peritoneal Mφs in lethally irradiated mice. Gating strategies identifying lymphoid and myeloid cell populations in **(A)** peritoneum and (**B**) spleen. FACS-purified early pro-B cells containing a bi-phenotypic pB-Mφ^{precursors} and mature B cells (control) from bone marrow of *Mb1*-iCre/Rosa26-*YFP* mice (see suppl. Fig. 6.1) were mixed in ratio 1:10 with total bone marrow cells from congenic CD45.1 donor mice and injected i.v. into lethally irradiated (9.5 Gy) wild type mice. Haematopoietic reconstitution was assessed in peritoneum and spleen at 2 and 4 weeks post injection of donor bone marrow cells. (**C**) Representative plots showing engraftment of donor CD45.1^{+} (all lineages) and YFP^{+} (early pro-B/mature B) cells in the peritoneum of lethally irradiated mice at 2 and 4 weeks post adoptive cell transfer.

Supplementary Figure 7.1

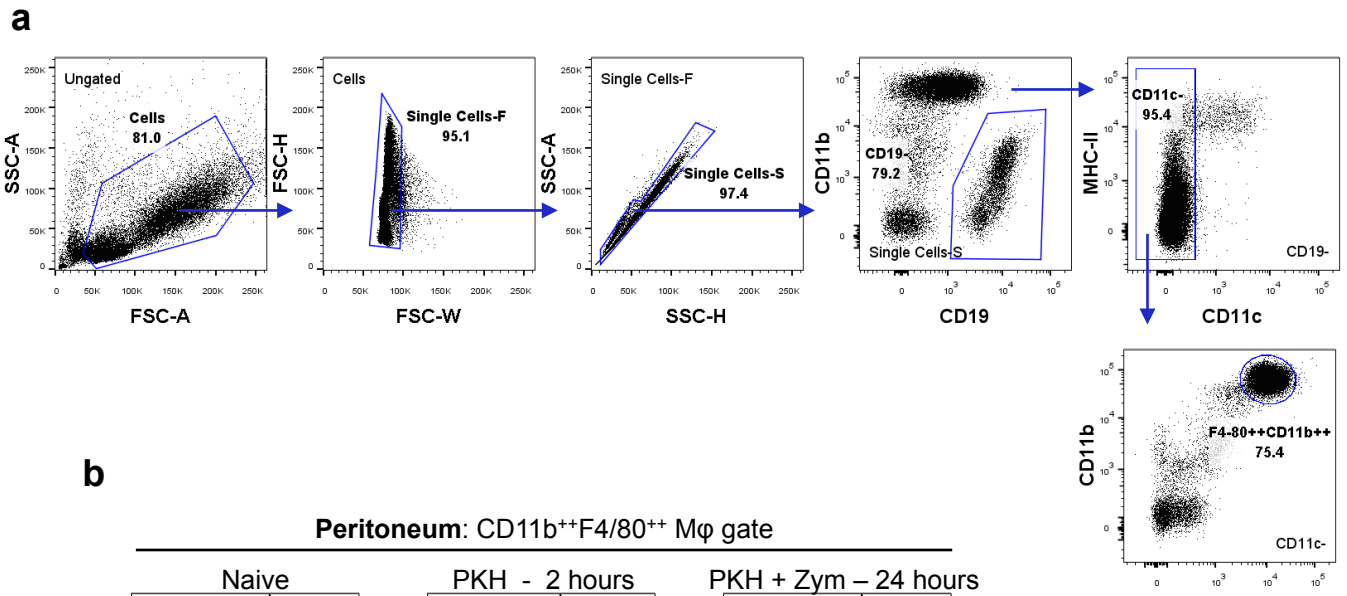

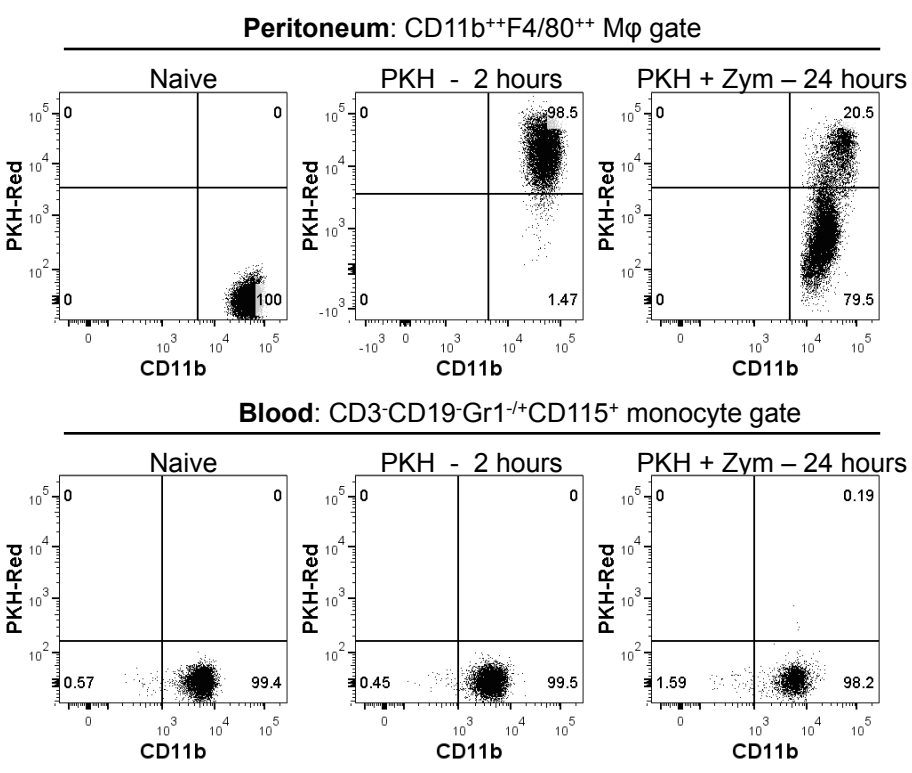

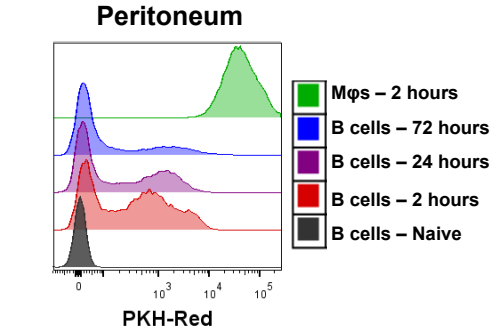

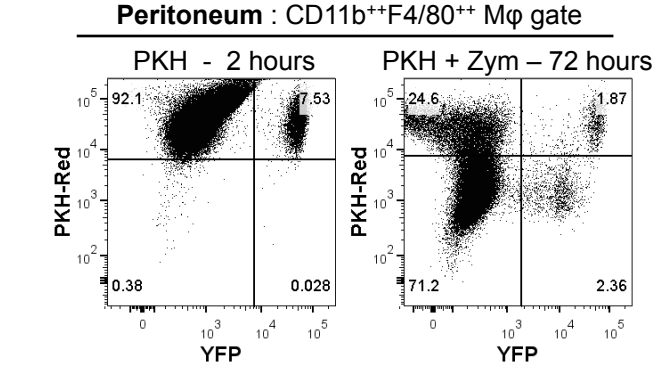

Supplementary Figure 7.1. PKH-Red labelling distinguishes between resident and inflammation-induced populations of peritoneal Mφs. To label resident peritoneal Mφs in contrast to infiltrating monocytes and inflammation-induced Mφs, phagocytic dye PKH-Red was injected i.p. 2 hours prior to zymosan administration. **a**, Gating strategy for identification of peritoneal Mφs. **b**, Peritoneal and peripheral blood leukocyte populations were analysed by flow cytometry. $CD11b^{++}F4/80^{++}$ peritoneal Mφs revealed bright and homogenous labelling after 2 hours post PKH-Red injection being a result of phagocytic ingestion of the dye, while no $CD3^{-}CD19^{-}Gr1^{-/+}CD115^{+}$ blood monocytes were labelled by PKH-Red at any time. Animals that received PKH-Red and zymosan (PKH + Zym) i.p. revealed $PKH\text{-}Red^{+}$ (resident) and $PKH\text{-}Red^{-}$ (inflammation-induced/monocyte-derived) populations within $CD11b^{++}F4/80^{++}$ Mφ gate. **c-d,** Due to their phagocytic ability $CD19^{+}$ B cells acquire some PKH-Red signal, which is however significantly lower than PKH-Red labelling of resident Mφs (**b, c**), including YFP^{+} Mφs present in naïve cavity and at 72 hours (**d**). This allows discrimination between PKH^{+} pB-Mφs present in naïve peritoneum and $PKH^{-/low}$ pB-Mφs^{inflam} triggered from pro-B cells ($PKH\text{-}Red^{-/low}$) by inflammation detected by 72 hours of zymosan peritonitis in *Mb-1*.iCre/Rosa26-*YFP* mice (**d**).

Supplementary Figure 7.2

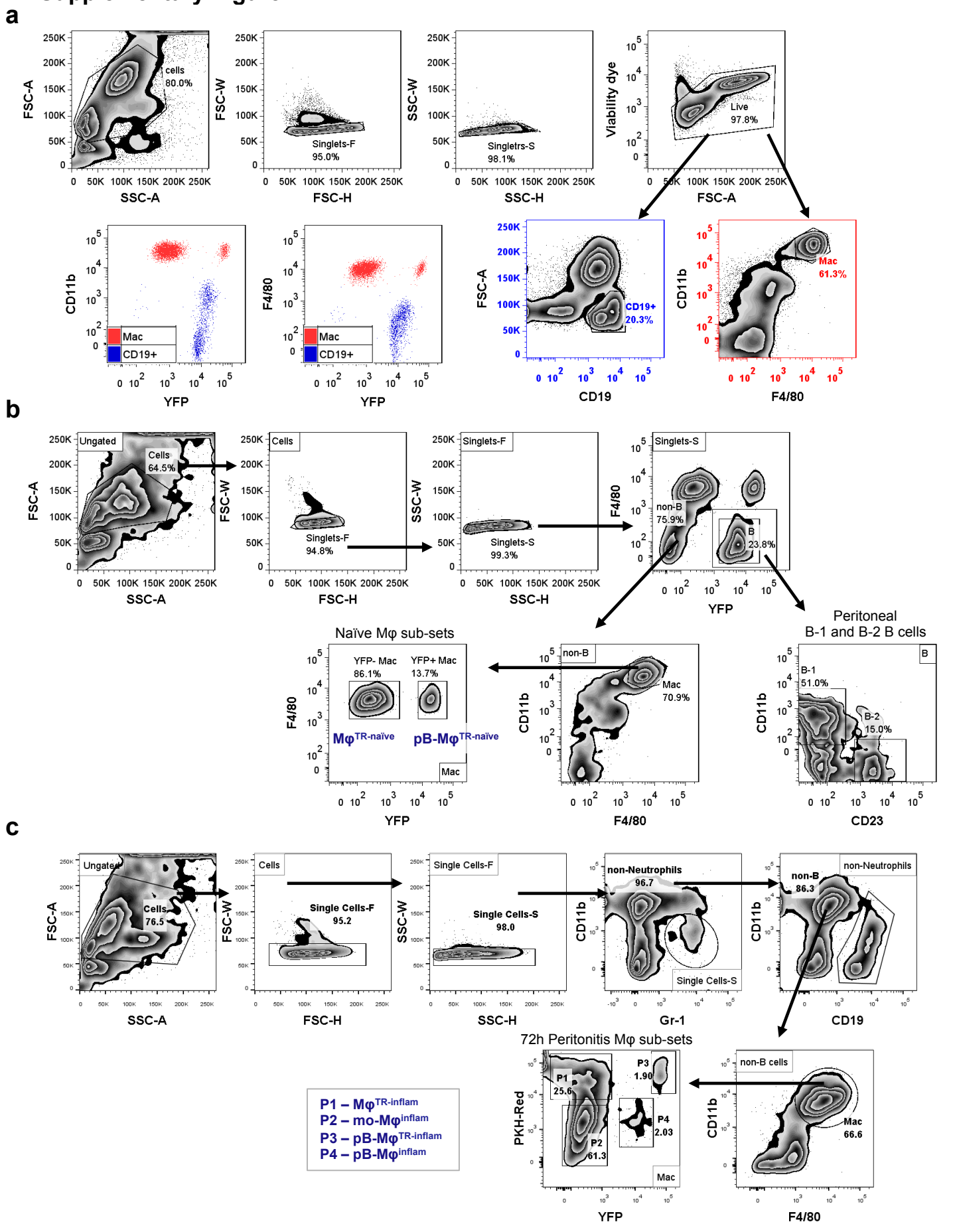

Supplementary Figure 7.2

d

Post-sort purity assessment : CD19^{+} B cell content in Mφ samples

Cell type	Mφ$^{TR\text{-}naïve}$			Mφ$^{TR\text{-}inflam}$			mo-Mφ^{inflam}			pB-Mφ$^{TR\text{-}naïve}$			pB-Mφ$^{TR\text{-}inflam}$			pB-Mφ^{inflam}		
Replicate #	**1**	**2**	**3**	**1**	**2**	**3**	**1**	**2**	**3**	**1**	**2**	**3**	**1**	**2**	**3**	**1**	**2**	**3**
B cells, %	0.78	0.42	3.72	0.43	0.00	0.64	0.00	0.00	0.20	7.04	3.54	3.46	1.39	0.00	3.12	6.9	10.1	3.1

Supplementary Figure 7.2. Gating strategy for isolation of Mφ and B cell sub-sets from *Mb1*-iCre/Rosa26R-*YFP* mice and post-sort purity assessment. a, CD19^{+} B cells and CD11b^{high}F4/80^{high} peritoneal Mφs identified among live single cells demonstrate YFP, F4/80 and CD11b expression levels characteristic for each cell type, i.e. high YFP, low/no F4/80 and no/intermediate CD11b expression on B cells; high F4/80 and CD11b on all Mφs with fraction of Mφ population expressing YFP. **b-c**, Gating strategies for FACS-purification of peritoneal Mφ populations and B cells from naïve peritoneum (**b**) and peritoneum at 72 hours post zymosan peritonitis induction (**c**). **d**, Mφ populations (n=3 per group) used for transcriptomic analysis were subjected to post-sort purity assessment. The content of contaminating B cells (YFP $^{+}$CD19^{+}) in FACS-purified Mφ samples, expressed in % from total Mφ sample.

Supplementary Figure 7.3

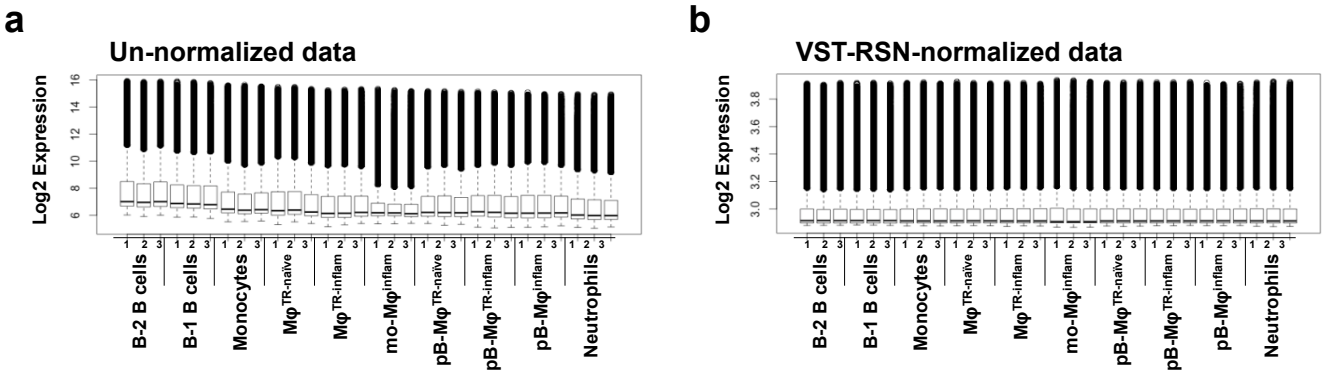

Supplementary Figure 7.3. Low variability across biological replicates of transcriptomic samlpes. Probe labelling and hybridization were performed using an Illumina *Mus musculus* 6v2 microarray (n=3 biological replicates). Array probe summaries were calculated in BeadStudio (Illumina) and subsequently normalized by a variance stabilising transformation (VST) and robust spline normalisation (RSN) using the lumi R/BioConductor package. **a-b,** Box plots of un-normalized (**a**) and normalized (**b**) expression data showing low variation within each sample group (n=3).

Supplementary Figure 7.4

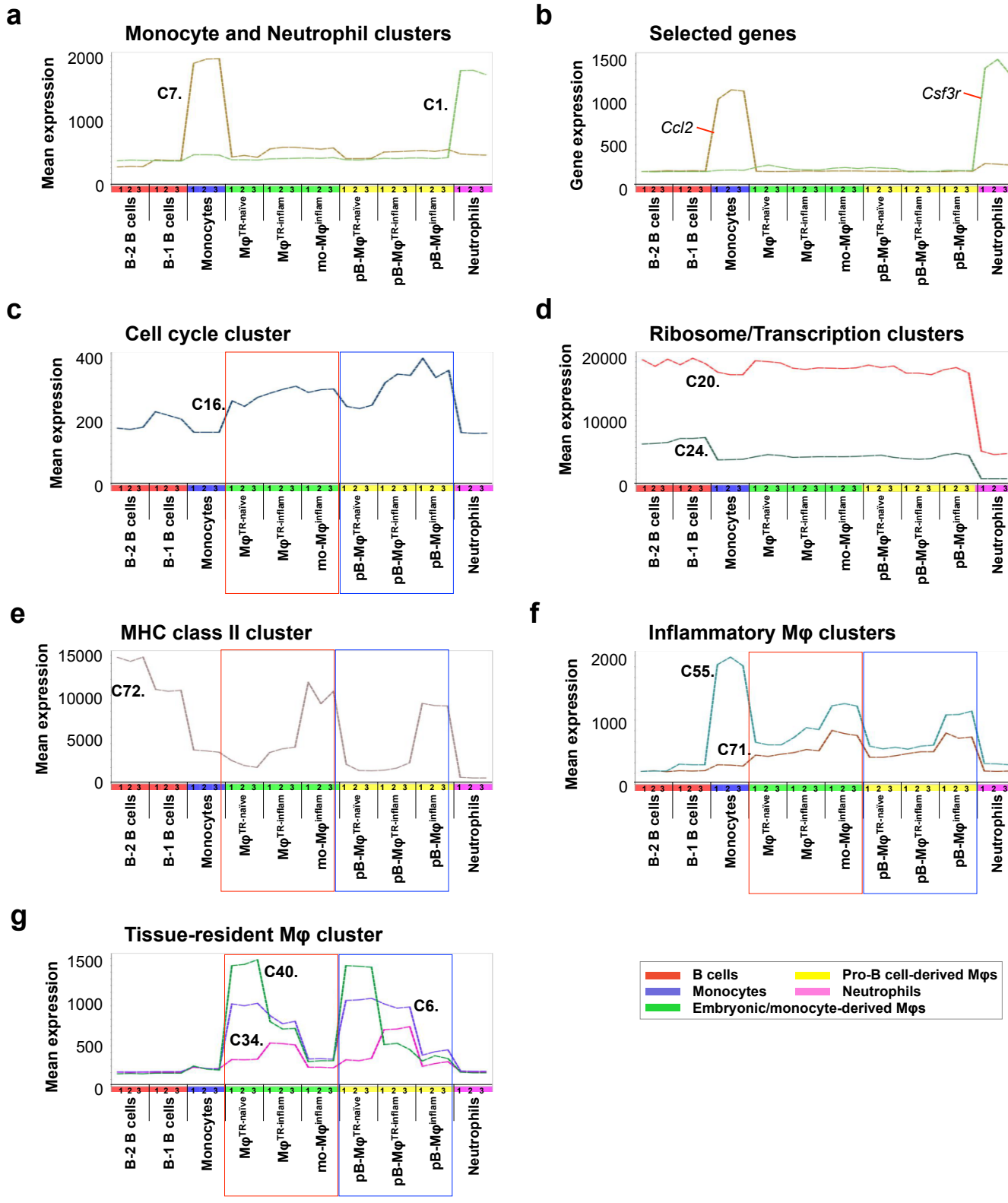

Supplementary Figure 7.4. Transcriptome analysis of pro-B cell-derived Mφs: expression profile of selected genes and gene clusters. The software tool Biolayout *Express*^{3D} was used for the visualization and analysis of Illumina *Mus musculus* 6v2 microarray data, which were variance stabilized (VST) and robust spline normalized (RSN) using the lumi R/BioConductor package. Full probeset-to-probeset Pearson correlation matrix was calculated in Biolayout *Express*^{3D} for each transcript represented on the array across the 30 samples using a correlation threshold of $r \geq 0.95$; MCL clustering algorithm with inflation value of 1.7 was used to generate gene clusters with similar functions or cell-specific activities. Expression profile of selected genes (**b**) or gene clusters **(a, c-g)** across all samples showing expression levels in pro-B cell-derived Mφs (blue rectangle) and embryonic/monocyte-derived Mφs (red rectangle). Mean expression levels of probe sets in monocyte-related cluster C7 and Neutrophil-related cluster C1 (**a**); Gene expression level of selected monocyte-related gene *Ccl2* and neutrophil-related *Csf3r* gene (**b**). Mean expression profiles of genes within cell-cycle-related gene cluster C16. (**c**); ribosomal and transcription-related gene clusters C20 and C24 (**d**) expressed highly by almost all cell populations except neutrophils; cluster C72 containing MHC class II genes expressed highly by B cells and both populations of inflammation-induced Mφs (**pB-Mφ^{inflam}/mo-Mφ^{inflam}**) (**e**). Genes highly expressed in inflammation-induced Mφs (**pB-Mφ^{inflam}/mo-Mφ^{inflam}**) in comparison to the other macrophage populations were found in clusters C55 and C71 (**f**), while clusters C6, C36 and C40 included genes characteristically expressed by tissue-resident Mφs from naïve (**pB-Mφ$^{TR\text{-}naïve}$/Mφ$^{TR\text{-}naïve}$**) and inflamed (**pB-Mφ$^{TR\text{-}inflam}$/Mφ$^{TR\text{-}inflam}$**) peritoneum (**g**).

Supplementary Figure 7.5

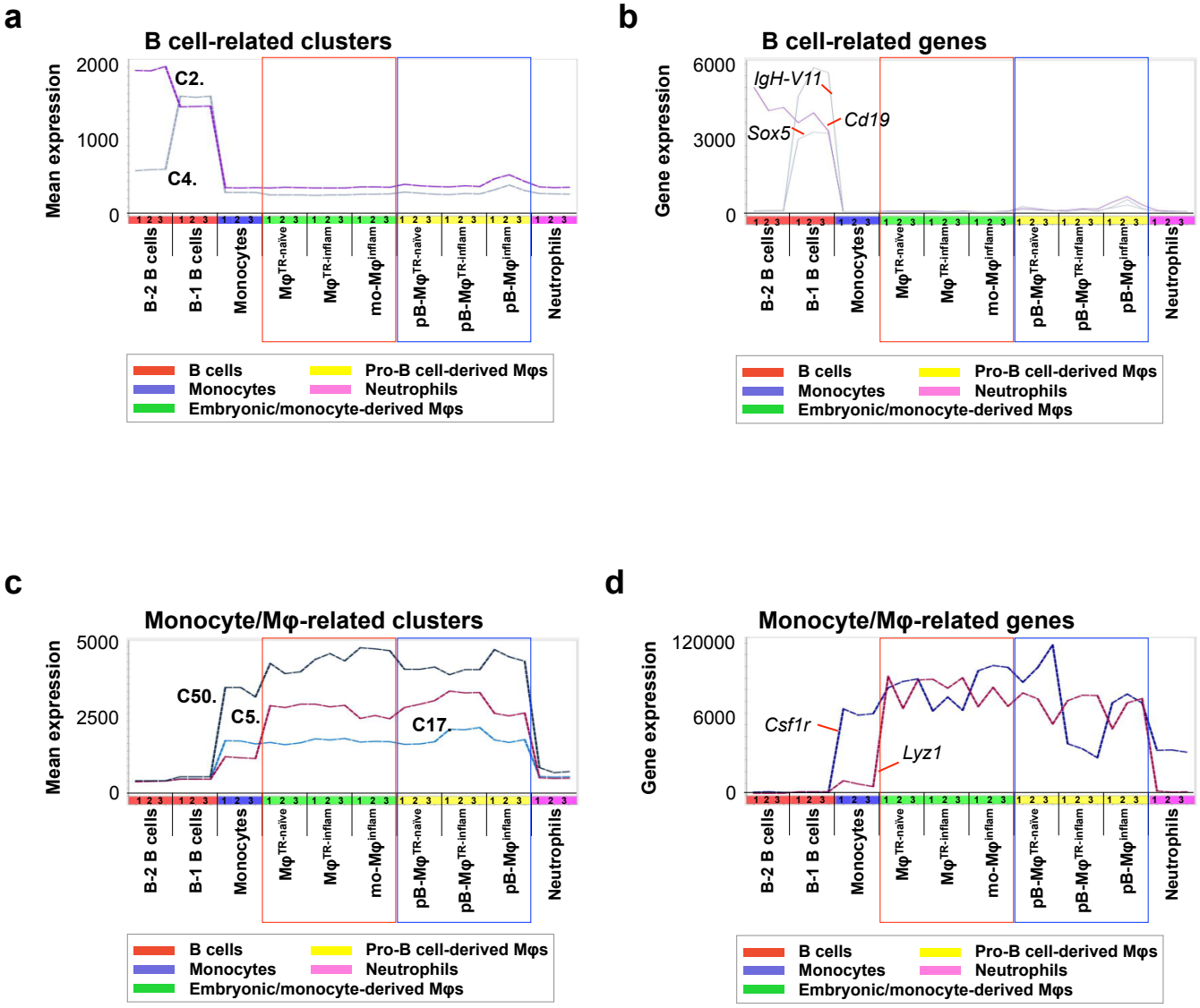

Expression profile of selected genes or gene clusters across all 30 datasets plotted in **a-c** showing expression levels for pro-B cell-derived Mφs (blue rectangle) and embryonic/monocyte-derived Mφs (red rectangle). Mean expression levels of probe sets in B cell-related clusters C2. and C4. **(a)** and Monocyte/Mφ-related clusters C5. C17, C50 **(c)**; Gene expression level of selected B cell-related genes *IgH-V11*, *Sox5* and *Cd19* **(b)** and Monocyte/Mφ-related genes *Csf1r* and *Lyz1* **(d)**. No clusters were identified, which contained genes which were expressed highly in pro-B cell-derived Mφs alone.

Supplementary data, Table S1

1) Spleen

	Day 7 % CD45.2	% eYFP in CD45.2	Day 14 % CD45.2	%eYFP in CD45.2
CD4 T cells	0.18 ± 0.14	0	5.03 ± 0.90	0
CD8 T cells	0.15 ± 0.08	0	2.59 ± 0.79	0
γδ T cells	0.12 ± 0.22	0	0.63 ± 0.31	0
NK cells	4.91 ± 3.12	0.80 ± 0.83	4.28 ± 2.01	0.38 ± 0.33
imm. B cells	29.94 ± 5.81	28.78 ± 4.57	13.95 ± 3.27	13.46 ± 2.84
T_1 B cells	5.86 ± 1.46	5.59 ± 1.75	18.68 ± 3.68	18.21 ± 3.87
T_2 B cells	2.98 ± 1.11	2.71 ± 1.13	7.56 ± 1.09	7.45 ± 1.46
T_3 B cells	0.77 ± 0.53	0.57 ± 0.36	8.92 ± 0.92	8.20 ± 0.60
Myeloid cells	49.35 ± 5.30	1.51 ± 0.45	17.33 ± 7.71	0.97 ± 0.55
Dendritic cells	2.39 ± 1.24	4.81 ± 9.83	2.41 ± 1.47	0.29 ± 0.17

2) Thymus

	Day 7 % CD45.2	% eYFP in CD45.2	Day 14 % CD45.2	%eYFP in CD45.2
ETP	64.88 ± 4.94	0.32 ± 0.11	2.15 ± 0.80	0.32 ± .023
DN2	11.17 ± 2.15	0.04 ± 0.09	6.62 ± 2.4	0.04 ± 0.03
DN3	4.29 ± 1.78	0	22.70 ± 8.63	0
DN4	1.00 ± 0.83	0	2.12 ± 0.68	0
DP	0.65 ± 0.75	0	48.24 ± 7.46	0
SP CD4	0.13 ± 0.17	0	4.54 ± 0.92	0
SP CD8	1.10± 0.71	0.62 ± 1.34	1.86 ± 0.57	0
γδ T cells	2.57 ± 1.10	0.02 ± 0.01	0.36 ± 0.06	0.01 ± 0.01
Dendritic cells	0.06 ± 0.08	0.01 ± 0.02	0.08 ± 0.06	0

3) Bone Marrow

	Day 7 % CD45.2	% eYFP in CD45.2	Day 14 % CD45.2	%eYFP in CD45.2
pro B cells	34.08 ± 4.71	33.70 ± 4.7	8.92 ± 3.78	8.64 ± 3.41
pre B cells	18.41 ± 5.48	18.47 ± 6.0	21.35 ± 9.71	20.94 ± 8.47
imm. B cells	8.40 ± 6.01	8.15 ± 5.47	8.58 ± 2.63	8.70 ± 2.58
mat. B cells	0.75 ± 0.94	0.79 ± 0.64	4.23 ± 0.30	4.19 ± 0.31
CLP	1.99 ± 1.31	0.28 ± 0.30	0.22 ± 0.32	0.05 ± 0.04
Myeloid cells	31.25 ± 12.09	1.62 ± 1.11	3.59 ± 2.52	0.19 ± 0.08

Transfer of 2 x 103 LMPP (B6.*Mb1*^{iCre}/*Gtrosa26*^{eYFP}) into CD45.1 *Rag2*-null (0.5 Gy irradiated) i.v.

Supplementary Materials and Methods

BCR re-arrangements detection and single cell PCR and RT-PCR

Sample preparation: FACS-purified single, 5, 10 or 20 cells were collected into wells of 96-well plates containing either 20 µl of lysis buffer A (1x DreamTaq™ DNA Polymerase Buffer (Thermo Scientific), 0.01% Gelatin (Sigma)) for PCR on genomic IgH locus; or 20 µl of lysis buffer B (1.25x of M-MVL Reverse Transcriptase Reaction Buffer (Promega), 0.4 units/µl of RNasin (Promega), 0.3125% Igepal (Sigma)) for reverse-transcription PCR and detection of B cell- and macrophage-specific mRNA transcripts. Plates were frozen on dry ice immediately after sort and stored at -80°C.

BCR re-arrangements detection by PCR: A multiplex PCR system was designed to amplify rearranged IgH genes from murine genomic DNA using nested PCR approach. Plates containg cells in 20 µl of lysis buffer A were thawed and briefly spun before addition of 1 µl of Protainase K (Invitrogen) to a final concentration of 400 µg/ml and then incubated in Thermocycler (TECHNE) for 60 min at 55°C, followed by 10 min incubation at 95°C. First PCR step was performed with 11 outer forward primers, each specific to a group of functional IgH_V genes, and 2 outer reverse primers specific to IgH_J genes (supplied by Sigma) (Table 1), using 0.125 µM of each primer, 3 µl of DreamTaq™ Buffer (1x), 0.25 µl of DreamTaq™ DNA Polymerase (Thermo Scientific), 1 µl of dNTPs (200 mM), 1 µl of 25mM $MgCl_2$ (2.5 mM) and 10 µl of 5x PCR enhancer (0.54 M Betaine, 1.34 mM DTT, 1.34% DMSO and 11 µg/ml BSA) per 50µl reaction, using the following PCR conditions: 2 min at 95°C, 30 cycles of 15 sec at 95°C, 30 sec at 59.5°C and 30 sec at 72°C, 10 min at 72°C on an Techne Thermocycler.

Table 1. Primer sequences used for IgH amplification (1st PCR amplification)

Primer ID	Primer sequence		T_{ann}	
VH-for1	GAGGTTCDSCTGCAACAGTY	Outer forward primers	59.5 °C	1st PCR Product size ~300-400 bp
VH-for2	CAGGTGCAAMTGMAGSAGTC			
VH-for3	GAVGTGMWGCTGGTGGAGTC			
VH-for5	GAKGTGCAGCTTCAGSAGTC			
VH-for7	CAGRTCCAACTGCAGCAGYC			
VH-for8	GAGGTGMAGCTASTTGAGWC			
VH-for11	CAGATKCAGCTTMAGGAGTC			
VH-for12	CAGGCTTATCTGCAGCAGTC			
VH-for13	CAGGTTCACCTACAACAGTC			
VH-for14	CAGGTGCAGCTTGTAGAGAC			
VH-for15	GARGTGMAGCTGKTGGAGAC			
JH-1_rev	CTTACCTGAGGAGACGGTGA	Outer reverse primers	59.5 °C	
JH-2_rev	CTTACCTGCAGAGACAGTGA			

Obtained PCR products were diluted 1:10 with H_2O and 1 µl was used for the second PCR reaction with 12 inner forward primers and 3 inner reverse primers (0.25 µM), using 2.5 µl of DreamTaq™ Green Buffer (1x), 0.125 µl of DreamTaq™ Green DNA Polymerase (Thermo Scientific), 0.5 µl of dNTPs (200 mM), 0.5 µl of 25mM $MgCl_2$ (2.5 mM) and 5 µl of 5x PCR enhancer (0.54 M Betaine, 1.34 mM DTT, 1.34% DMSO and 11 µg/ml BSA) per 25 µl reaction. PCR was performed using the following conditions: 2 min at 95°C, 30 cycles of 15 sec at 95°C, 30 sec at 59°C and 30 sec at 72°C, 10 min at 72°C on TECHNE Thermocycler. PCR products were analysed on 2% Agarose gel.

Table 1 (continued). Primer sequences used for IgH amplification (2nd PCR amplification)

Primer ID	Primer sequence		T_{ann}	
Inner_VH-for1	GGTTCDSCTGCAACAGTYWG	Inner forward primers	59.0 °C	2nd PCR Product size ~280-300 bp
Inner_VH-for2	GGTGCAAMTGMAGSAGTCWG			
Inner_VH-for3	GTGMWGCTGGTGGAGTCTGG			
Inner_VH-for5	GTGCAGCTTCAGSAGTCWGG			
Inner_VH-for5_2	GTGCAGCTTCAGSAGTCGRG			
Inner_VH-for7	CTGAGCTGGTGARRCCTGG			
Inner_VH-for8	GTGMAGCTASTTGAGWCTGG			
Inner_VH-for11	CAGATKCAGCTTMAGGAGTCWGGA			
Inner_VH-for12	CTGAGCTGGTGAGGC			
Inner_VH-for13	GTTCACCTACAACAGTCTGG			
Inner_VH-for14	GTGCAGCTTGTAGAGACCG			
Inner_VH-for15	TGMAGCTGKTGGAGACWGGA			
Inner_JH-1_rev	CCAGACATCGAAGTACCAGT	Inner reverse primers		
Inner_JH-2_rev	GCCTTGACCCCAGTAGTC			
Inner_JH-3_rev	GACAGTGACCAGAGTCCCTT			

Detection of B cell- and Mφ-specific mRNA transcripts by RT-PCR: Plates containg cells in 20 µl of lysis buffer B were thawed, briefly, spun, incubated at 70°C for 5 min and then cooled on ice. Random primers and Oligo$(dT)_{15}$ Primers were incubated at 70°C for 5 min and then cooled on ice before use. Reverse trancription reaction was performed on single and multiple cells using 1 µl of 500ng/µl Random Primers (Promega), 1 µl of 500 ng/µl Oligo$(dT)_{15}$ Primer (Promega), 2 µl of 10 mM dNTPs and 0.5 µl M-MLV Reverse Transcriptase per 25 µl reaction using the

following conditions: 5 min at 25°C, 60 min at 40°C and 10 min at 75°C. PCR amplification was performed using 10 µl of cDNA, 0.625 µl of forward and reverse *Emr1* or *Cd79b*-specific primers (0.25 µM) (see Table 2), 2.5 µl of DreamTaq™ Green Buffer (1x), 0.125 µl of DreamTaq™ Green DNA Polymerase (Thermo Scientific), 0.5 µl of dNTPs (200 mM) and 0.75 µl of DMSO (3%) per 25µl reaction using the following conditions: 2 min at 95°C, 49 cycles of 15 sec at 95°C, 20 sec at specified annealing temperature (see Table 2) and 30 sec at 72°C, 10 min at 72°C on Techne Thermocycler. PCR products were analysed on 4% Agarose gel.

Using PCR methods described above the following cell populations from naïve peritoneum were examined: B-1 B cells ($CD19^+$ $CD23^-$ $CD11b^+$ $Gr1^-$ $F4/80^-$) and B-2 B cells ($CD19^+$ $CD23^+$ $CD11b^-$ $F4/80^-$), naïve $CD19^+$ and $CD19^-$ pro-B cell-derived macrophages ($F4/80^{high}$ $CD11b^{high}$ YFP^+), as well as yolk sac macrophages ($F4/80^{high}$ $CD11b^{high}$ YFP^-) purified from B6.*Mb1*-iCre/Rosa26-*YFP*. At least 45 wells containing either single or multiple cells per well were analyse for each cell type.

Table 2. Primer sequences used for RT-PCR

Primer ID	**Primer sequence**	**T_{ann}**	**Product size, bp**
Emr1_for	GGAAGCCTCGTTTACAGGTG	56.4°C	150
Emr1_rev	GGATGTACAGATGGGGGATG		
Cd79b_for	GCTTTTTGGCTGCAAACCT	54.1°C	95
Cd79b_rev	GGTACCAGCAATGACAAGCA		

Microarray analysis

RNA was extracted from FACS-purified murine peritoneal cells populations using RNAZol (Moleclular Research Center, Inc.) and normalised to equal mass. Cell surface markers and relevant gating strategies used for cell purification are shown in Table 3 below and Fig. S15. Probe labeling and hybridization were performed using

an Illumina *Mus musculus* 6v2 microarray as per manufacturer's instructions. The array probe summaries for 30 datasets (n=3 per group) were calculated in BeadStudio (Illumina) and subsequently normalised by a variance stabilising transformation (VST) (1) and robust spline normalisation (RSN) using the lumi R/BioConductor package (2) (Fig. S16). Significantly differentially expressed genes were identified using the limma R/BioConductor package (3) to generate linear models for normalized probe intensity data, applying multiple *t*-tests between groups of sample replicates and selecting probes which gave Benjamini-Hochberg adjusted P-values < 0.001. Genes with very low or no expression among all samples compared were filtered out based on P-detection-value (> 0.01). Correlation analysis of the gene expression profiles of the individual cell populations and identification of co-expression modules were performed in Biolayout *Express*^{3D} (4). The global gene expression profiles of the individual cell populations were compared using Pearson correlation threshold of $r \geq 0.97$ in order to analyse the similarity between samples. A full probeset-to-probeset Pearson correlation matrix was calculated in Biolayout *Express*^{3D} for each transcript represented on the array across the 30 samples using a correlation threshold of $r \geq 0.95$. The graph was clustered using the MCL algorithm with an inflation value of 1.7 to generate clusters of genes with similar cell-specific activities. The network graph contained 11,216 nodes (probe sets representing specific transcripts) and after MCL-clustering (1.7) generated 272 distinct clusters containing ≥ 6 probe sets. The graph's structure is presented in Fig. 6C. The microarray data are publicly available in ArrayExpress, accession number: E-MTAB-1878.

Table 3. Cell surface markers used for cell sorting

Cell type	Sorting strategy	Source	
Follicular B-2 B cells	$B220^{+}$ $CD23^{high}$ $CD21^{low}$	Spleen	C57BL6 mice
Peritoneal B-1 B cells	$CD19^{+}$ $CD23^{-}$ $CD11b^{int}$ $F4/80^{-}$	Peritoneum	
Peritoneal B-2 B cells	$CD19^{+}$ $CD11b^{-}$ $CD23^{+}$ $F4/80^{-}$	Peritonitis 4h	
Monocytes 16h	$CD19^{-}$ $CD115^{+}$ $Gr1^{int}$	Peritonitis 16h	
Neutrophils 16h	$CD19^{-}$ $CD115^{-}$ $Gr1^{high}$ $CD11b^{+}$	Peritonitis 16h	
Naïve B-1/Mφs	$CD19^{-}$ $F4/80^{high}$ $CD11b^{high}$ YFP^{+}	Peritoneum	B6.*Mb1*-iCre/ Rosa26-*YFP* mice
$M\varphi^{TR\text{-}naïve}$	$CD19^{-}$ $F4/80^{high}$ $CD11b^{high}$ YFP^{-}	Peritoneum	
mo-$M\varphi^{inflam}$	$CD19^{-}$ $F4/80^{high}$ $CD11b^{high}$ YFP^{-} PKH-Red^{-}	Peritonitis 72h + PKH-Red	
$M\varphi^{TR\text{-}inflam}$	$CD19^{-}$ $F4/80^{high}$ $CD11b^{high}$ YFP^{-} PKH-Red^{+}		
pB-$M\varphi^{inflam}$	$CD19^{-}$ $F4/80^{high}$ $CD11b^{high}$ YFP^{+} PKH-Red^{-}		
pB-$M\varphi^{TR\text{-}inflam}$	$CD19^{-}$ $F4/80^{high}$ $CD11b^{high}$ YFP^{+} PKH-Red^{+}		

H**ematopoietic cell isolation**

Peritoneal cells were obtained by lavage with 2 ml of PBS-based cell dissociation buffer (Invitrogen). Cells were centrifuged at 750 g for 4 min at 4°C and then red blood cells were depleted by incubation with 0.2 ml ACK lysing buffer (Lonza). Lysis was stopped by addition 1 ml of 1% FCS 2 mM EDTA in PBS (FACS Buffer) and subsequent centrifugation. Cells were washed once more with 1 ml of FACS buffer and counted. Pleural cavity cells very harvested and processed similarly. Spleens were crushed between two glass slides in cold RPMI supplemented with 10% FSC and 100 units/ml of penicillin and 100 µg/ml of streptomycin (Invitrogen), obtained crude cell suspension was vigorously mixed by pipetting, passed through 70 µm cell strainer (BD Falcon) and centrifuged. Red blood cell lysis was performed as above

using 4-5 ml of ACK buffer/spleen. Bone marrow cells were purified from femurs and tibiae, which were cleaned from surrounding muscle tissues, dipped in 70% ethanol for 0.5-1 min for disinfection. Then both ends of the bone were cut with scissors and the marrow flushed with 1% FCS 2 mM EDTA in PBS/RPMI using a syringe with a 26G needle. Clusters within the marrow were disintegrated by vigorous pipetting. Red blood cells were lysed as above. Incubation with 10x volume of ACK lysing buffer (Lonza) was employed for peripheral blood cells purification, which was followed by washing with PBS and FACS Buffer. Small and large intestines were dissected from mice, washed of faecal content with cold HBSS and opened longitudinally. Tissue was then cut in 0.5 cm pieces and incubated twice in 5 ml of 5% FCS, 2 mM EDTA, 1 mM DTT in HBSS for 20 min at 37^{o}C on shaker (220 rpm) to remove epithelial cells. Then tissue was briefly washed with cold PBS and digested with 1.5 mg/ml Collagenase VIII (Sigma), 0.5 mg/ml DNase I (Sigma) and 1 mg/ml Dispase II (Sigma) in Dulbecco's PBS with Mg^{2+} and Ca^{2+} for 20 min at 37^{o}C on shaker (220 rpm). After complete digestion cells were strained through 70 μm mesh and centrifuged. Cells were washed once more with 1% FCS 2 mM EDTA in PBS prior use. For brain and liver mononuclear cells analysis animals were perfused with 30 ml PBS via the left ventricle. Brain and liver were collected; tissues were sectioned and homogenized using a dounce homogenizer to obtain cell suspensions, which were filtered through 70 μm mesh and spun. Pellets were re-suspended in 5 ml of 30% percoll, laid over 5 ml 70% percoll and centrifuged at 1000 g for 20 min at 20ºC with low acceleration and no brake. Cells from interphase were collected using Pasteur pipette washed once in PBS and analysed by flow cytometry.

Clonal assay

S17 stromal cell lines were maintained in Iscove's modified Dulbecco's medium with 20% (vol/vol) FCS, seeded into 96 well flat bottomed plates and were irradiated with

30 Gy at 80% confluency. 24 h later, cells were washed and supplemented with 10% (vol/vol) FCS, 0.1 mM βmercaptoethanol and media containing growth factors for myeloid development (SCF [100ng/ml], Flt3L [5ng/ml], M-CSF [100ng/ml] and anti-IL7 Ab [3µg/ml]) or lymphoid development (SCF, Flt3 and IL7 [10ng/ml]). Growth factors were from Peprotech with IL7 neutralizing antibody from R&D Systems. Cells were sorted directly onto the stromal layers and were incubated for 10–14 d at 37 °C in 7.5% CO_2, followed by flow cytometry. CD11b, Gr1, F4/80 and CD45 were used to discern myeloid cells while B220, CD19 and IgM were used for lymphoid cells.

REFERENCES

1. Lin SM, Du P, Huber W, & Kibbe WA (2008) Model-based variance-stabilizing transformation for Illumina microarray data. *Nucleic Acids Res* 36(2):e11.
2. Du P, Kibbe WA, & Lin SM (2008) lumi: a pipeline for processing Illumina microarray. *Bioinformatics* 24(13):1547-1548.
3. Smyth GK (2004) Linear models and empirical bayes methods for assessing differential expression in microarray experiments. *Statistical applications in genetics and molecular biology* 3:Article3.
4. Freeman TC*, et al.* (2007) Construction, visualisation, and clustering of transcription networks from microarray expression data. *PLoS computational biology* 3(10):2032-2042.